



DR. SEKAR NAGAIYAN NETHI (Orcid ID : 0000-0001-7568-5129)

Article type : Research Article

# NLOphoric Triphenylamine Derived Donor- $\pi$ -Acceptor- $\pi$ -Donor Based Colorants: Synthesis, Spectroscopic, Density Functional Theory and Z-scan Studies

Manish M. Raikwar,<sup>1</sup> Elizabeth Mathew,<sup>2</sup> Manu Varghese,<sup>2</sup> Issac H. Joe,<sup>2</sup> and Nagaiyan Sekar\*

<sup>1</sup>*Department of Dyestuff Technology, Institute of Chemical Technology, (Formerly UDCT), Nathalal Parekh Marg, Matunga, Mumbai, 400019, India.*

<sup>2</sup>*Centre for Molecular and Biophysics Research, Department of Physics, Mar Ivanios College, Thiruvananthapuram, Kerala 695015, India.*

*Corresponding author's email: n.sekar@ictmumbai.edu.in, nethi.sekar@gmail.com*

## Abstract

Three Donor- $\pi$ -Acceptor- $\pi$ -Donor type styryl dyes (**5a-c**) with different secondary donors are synthesized and characterized to study their non-linear and linear optical properties. The structure-property relationships of the dyes are described in the light of systematic photophysical and theoretical investigations. The photophysical characteristics of **5a-c** are influenced by the polarity of the medium, with an appreciable bathochromic shift in emission

This article has been accepted for publication and undergone full peer review but has not been through the copyediting, typesetting, pagination and proofreading process, which may lead to differences between this version and the Version of Record. Please cite this article as doi: 10.1111/php.13089

This article is protected by copyright. All rights reserved.

(**5b** = 81 nm) and large Stoke shifts (**5b** = 104-173 nm) in polar solvents. **5a-c** showed intramolecular charge transfer characteristics recognized with the help of emission solvatochromism, solvent polarity graphs, natural bond orbital analysis, and HOMO-LUMO energy difference. The optimized geometry and frontier molecular orbitals reveal that the electron donation takes place from secondary donors and not from a fixed donor (triphenylamine) which is more twisted. The non-linear optical properties obtained using solvent induced spectral shift and computational methods are found within the limiting values. Z-scan results reveal saturable kind of behavior for **5a**, **5b**, and **5c**, whereas **5a** and **5b** show reverse saturable kind of behavior in acetone and ethanol and hence give optical limiting values. The two photon absorption cross-section described by two level approximation is highest for **5b** (251-300 GM).

**Keywords:** Donor, Acceptor, Triphenylamine, Dicyano vinylene, Solvatochromism, DFT, NLO, Z-scan

---

## Introduction

In past few decades, there is notable progress in the design and development of functional materials as promising candidate for applications in bio-sensing fluorescence technology (1), electroluminescence devices (2), non-linear optics (NLO) (3, 4), organic light emitting diodes (OLED) (5, 6), photoconductors (7, 8), photovoltaic (9, 10), solid-state lasers (11, 12), thin film transistors (13–15), two photon absorption materials (TPA). Push-pull dyes are organic molecules containing Donor- $\pi$ -Acceptor (D- $\pi$ -A) framework where donor and acceptor are linked through conjugated  $\pi$ -bonds. They are easy to synthesize and their properties can be improved based on the nature of the donor, acceptor or  $\pi$ -linker used (16). Besides the typical linear D- $\pi$ -A arrangement, the recent trend in the design includes

quadrupolar (D- $\pi$ -A- $\pi$ -D or A- $\pi$ -D- $\pi$ -A) (17, 18) and octupolar (tripodal) (D- $\pi$ -)<sub>3</sub>A or (A- $\pi$ -)<sub>3</sub>D (19–21). Recently organic fluorophores with D- $\pi$ -A- $\pi$ -D received interest in organic electronics, on account of intramolecular charge transfer (ICT) improved light absorbance (22–24). As these molecules give broad range absorption spectra resulting in the reduced energy difference between the HOMO and LUMO. This can be achieved by tuning the HOMO and LUMO via suitable choice of electron donor and electron acceptor units in the organic fluorophores (25, 26). Further, the relationship between the different donor and acceptor groups and their influence on photophysical and electrochemical properties can be studied (27, 28).

Over the years, push-pull organic dyes with highly resonating and polarizable  $\pi$ -electron framework are used as second and third-order non-linear materials (29–31). This is because organic molecules employed in NLO applications unlike inorganic molecules offer numerous advantages such as well-defined structure, ease of synthesis and tenability, and large optical non-linearities and responses. The donor-acceptor units attached to the  $\pi$ -conjugated system are known to play a crucial role in terms of NLO activity. Thus, by increasing the donor-acceptor strength of a system can lead to enhanced non-linearity (32). The non-linear optical responses of the push-pull molecular system is related to ICT from donor to acceptor through a  $\pi$ -conjugated network. Designing new systems with excellent charge transfer (CT) plays a vital role as improved ICT will further enhance the NLO susceptibility for the designed molecule (33). Dipolar (D- $\pi$ -A)(34, 35), quadrupolar (D- $\pi$ -A- $\pi$ -D or A- $\pi$ -D- $\pi$ -A) (32, 36–38) or octupolar systems (39–41) are widely investigated for the applications as NLO materials. As the CT in such systems describes the low energy physics of these molecules and is also responsible for low-energy excitations with the large transition and/or mesomeric dipole moments (42). Quadrupolar molecules with the D- $\pi$ -A- $\pi$ -D framework are also known to exhibit excellent third order NLO properties (43–45). Second-

order materials NLO materials are being used in green lasers acquired through frequency doubling of the red sources, second-harmonic generation microscopy and terahertz wave generation (44, 46, 47).

Herein, we report the design and synthesis of fluorescent three styryl dyes with the D- $\pi$ -A- $\pi$ -D framework. The strategy involved in this study is to keep one donor fixed as triphenylamine whereas varying the secondary donor having different  $\pi$ -conjugated network and acceptor as dicyano vinylene group so as to ascertain the effect of varying secondary donor on the photophysics of the dyes. Triphenylamine due to its excellent electron donating ability and CT characteristic is utilized in numerous molecular design for a variety of applications. The coplanarity between the central nitrogen atom and the three rings allows an uninterrupted conjugation of the lone pair electrons with the electrons in the aromatic ring thereby increasing the  $\pi$ -electron density of the system. Hence, triphenylamine not only helps in increasing the solubility but also the electron donating ability and the extent of  $\pi$ -delocalization (48–51). This outstanding property of triphenylamine marks it as a suitable fixed primary donor for our study. Introduction of an accepting group has found to enhance the ICT capabilities of triphenylamine (52–55). Here dicyanovinylene group is used as an acceptor as it offers several advantages like providing highly polar structures and helps in tuning the photophysical and electrochemical properties as well (56–58). We expect these dyes to show enhanced photophysical and NLO properties as compared to previously reported analogous **1** (59). As **1** is a dipolar molecule with only one donor whereas these synthesis styryl dyes have a D- $\pi$ -A- $\pi$ -D framework with the secondary donor, which we expect will help to enhance the optical and NLO properties of the synthesized styryl dyes in comparison with the known NIR emitting **1**. These styryl dyes were prepared by the condensation of 2-(1-(4-(diphenylamino)phenyl)ethylidene)malononitrile with different aldehydes in ethanol using piperidine as base and were characterized by  $^1\text{H}$  NMR and  $^{13}\text{C}$

NMR. Photophysical properties of these dyes were investigated in solvents of increasing polarity. Further, their structural, photophysical and NLO properties were investigated using DFT and TD-DFT computations.

<FIGURE 1>

## Materials and Methods

*Material and equipments.* All the reagents were obtained from Sigma Aldrich, Alfa Aesar, Spectrochem and S. D. Fine Chemicals and used as supplied without any further purification. All the solvents used were of spectroscopic grade procured from Merck. The reactions were monitored by TLC using 0.25mm E-Merck silica gel 60 F<sub>254</sub> precoated plates. <sup>1</sup>H NMR and <sup>13</sup>C NMR spectra were recorded on Varian 500-MHz instrument (USA) using CDCl<sub>3</sub> solvent and TMS as an internal standard at 25 °C. The chemical shifts were reported in parts per million (ppm) relative to the internal standard as tetramethylsilane (TMS). The absorption spectra were recorded on Perkin Elmer Lambda 25 UV-Visible spectrophotometer and emission spectra on Varian Inc. Cary Eclipse spectrofluorometer.

*Computational details.* The molecular geometries of **5a-c** were optimized using DFT computations using the Gaussian 09 program (60). The ground state (S<sub>0</sub>) geometry of these dyes was optimized in the gas phase as well as in the solvent environment of varying polarity using self-consistent reaction field (SCRF) incorporated in polarizable continuum model (PCM) (61, 62) as implemented in Gaussian 09 (63). The functional used was B3LYP, it is the method that combines Becke's three parameter exchange functional (B3) (64) with the nonlocal correlation functional by Lee, Yang and Parr (LYP) (65). The basis set used for all atoms was 6-311++G(d,p) (66). The excited state optimization was carried out using time-dependent density functional theory (TD-DFT). The excitation energies, oscillator strengths

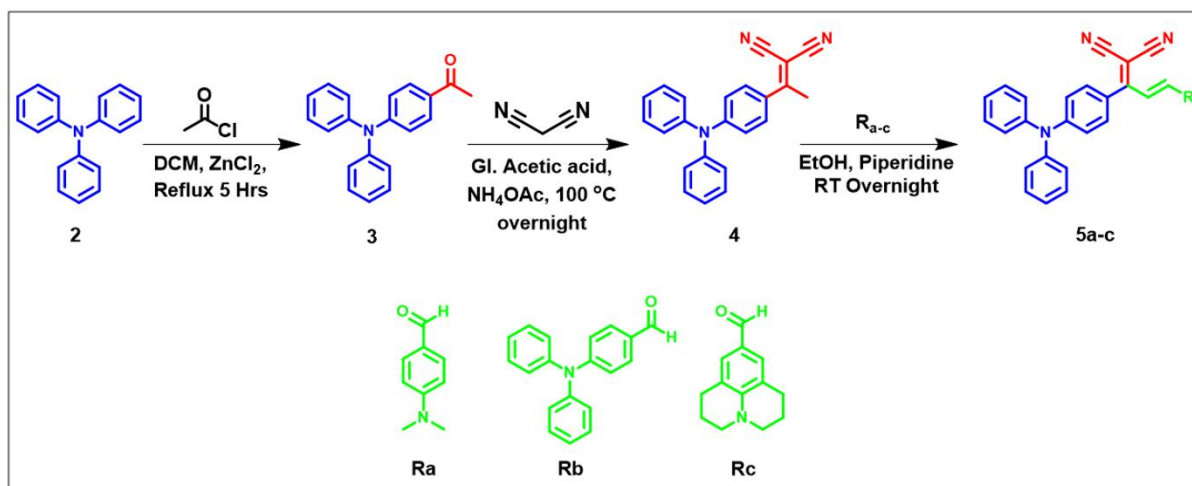
and orbital contribution for the lowest 10 singlet-singlet transitions at the optimized geometry were obtained by TD-DFT (67, 68) calculations using the same basis set as for the geometry minimization. The solvents used were toluene, dichloromethane (DCM), 1,4-dioxane, ethyl acetate (EtOAc), acetone, *N,N*-dimethyl formamide (DMF), and dimethyl sulfoxide (DMSO). The NLO parameters were calculated using global hybrid (B3LYP) and range separated hybrid functional (CAM-B3LYP) with the basis set 6-311++G(d,p) for comparison.

*Z-scan measurements.* The third-order NLO properties of the synthesized styryl dyes were measured using the Z-scan technique. It is an effective and popular technique for the accurate measurements of nonlinear refractive index ( $n_2$ ), nonlinear absorption coefficient ( $\beta$ ) and third-order nonlinear optical susceptibility ( $\chi^{(3)}$ ). The open and closed aperture Z-scan measurements were carried out using a pulsed neodymium-doped yttrium aluminium garnet (Nd:YAG) laser having 5 ns pulses at a repetition rate of 10 Hz giving second harmonic at 532 nm. The sample was moved in the direction of propagation of light focused with a lens of focal length 10 cm. The radius of the beam waist was calculated to be 35 mm. The Rayleigh length,  $z_0 = \pi\omega_0^2/\lambda$  was calculated as 7.42 mm which is greater than thickness of the sample cuvette (1 mm), an essential requirement for Z-scan experiments. The transmitted beam energy, reference beam energy and their ratio are measured simultaneously by an energy ratio meter having two identical detector heads. The optical limiting behaviour was studied without aperture under Nd:YAG laser (532 nm) illumination in acetone and ethanol solvent media. In this experiment, the sample probe is placed at the focal plane of the lens. A neutral density filter is used to vary the input fluence (or energy) and the transmitted fluence after passing through the sample is recorded using a photo-detector. The laser damage threshold values were measured using Nd:YAG laser (532 nm) with a repetition rate of 10 Hz and a

pulse width ( $t$ ) of 5 ns. The dyes were placed at the focus of a plano-convex lens of focal length ( $f$ ) 10 cm.

Two-photon absorption (2PA) cross section ( $\sigma_{2PA}$ ) is described by two-level model using solvatochromic data, the details of which is described in the supporting information.

*Design and Synthesis.* The synthetic scheme for the synthesis of the dyes **5a-c** with the D- $\pi$ -A- $\pi$ -D framework is illustrated in Scheme 1. The parent chromophore, 1-(4-(diphenylamino)phenyl)ethan-1-one (**3**) was synthesized by the acylation of triphenylamine by slightly modifying the procedure as described in the literature (69). The Knoevenagel condensation of **3** with malononitrile using a catalytic amount of ammonium acetate yielded 2-(1-(4-(diphenylamino)phenyl)ethylidene)malononitrile (**4**) (70). Aldehydes **R<sub>a</sub>**, **R<sub>b</sub>**, and **R<sub>c</sub>** were procured from the commercial sources. Final condensation of the respective aldehydes with intermediate **4** resulted in styryl dyes **5a**, **5b**, and **5c**. The dyes were fully characterized by nuclear magnetic resonance ( $^1\text{H}$  and  $^{13}\text{C}$  NMR) spectroscopy as well as the elemental analysis and the spectral data are consistent with the proposed structure. The dyes **5a**, **5b**, and **5c** possessed brick red, orange and greenish golden color respectively, and are soluble in common organic solvents like toluene (TOL), dichloromethane (DCM), ethyl acetate (EtOAc), acetone, N,N-dimethylformamide (DMF), dimethyl sulfoxide (DMSO) but sparingly soluble in ethanol (EtOH) and methanol (MeOH). The modified procedures for the intermediates along with the analytical characterization is given in supporting information.



**Scheme 1.** Synthesis route for the styryl dyes **5a-c** from the intermediate **4**.

## Result and discussion

### Photophysical properties

Absorption and fluorescence spectroscopy was used to investigate the photophysical properties of the dyes. **Figure 2(a)** displays the absorption spectra of the dyes recorded in toluene and the relevant data are presented in **Table 1**. All the dyes exhibit two distinct absorption maxima in the range 280–525 nm. The shorter wavelength absorption maxima seen below ~340 nm are allocated to the various localized  $\pi$ - $\pi^*$  electron transitions arising from chromophores, in particular, triphenylamine, phenyl, and julolidine, (71, 72) which fuse together in the majority of dyes. The lower energy absorption peak observed in the wavelength range, 472–523 nm is inevitably seen in all the dyes and are assigned to ICT transition from the attached chromophores (D<sub>2</sub> donor) to the dicyanovinylene acceptor. Nature of the chromophores, its electron donating tendency and the position of their attachment have considerable influence on the absorption wavelength and molar absorptivity of the dyes. Therefore, the absorption maximum for **5a-c** in toluene is observed at around 472 nm, 479 nm, and 523 nm respectively. The dyes show a red shifted absorption maxima, with the escalation in the electron donating tendency of a D-A fragment in the order **5c** > **5b** > **5a**

(Table 1) which is a characteristic behaviour of ICT bands. Dyes **5a** and **5b** have a freely rotating *N*-alkyl/aryl donors that directly affect the planarity of the system. On the contrary, **5c** with a rigid donor (julolidine) has higher planarity in the system. So, we observe here that the peak wavelengths of the absorption band are in order **5c** > **5b** > **5a**. Thus, for **5c**, the red shifted absorption observed is accredited to the rigid planar framework resulting in effective delocalization of the  $\pi$  – electron between the D<sub>2</sub> donor (julolidine group) and acceptor (dicyano vinylene group) and +I effect of julolidine.

<FIGURE 2>

**Table 1.** Observed photophysical parameters of **5a-c** in toluene.<sup>[a]</sup>

Dyes	<sup>[b]</sup> $\lambda_{\text{abs}}$ (nm)	<sup>[c]</sup> $\epsilon_{\text{max}} \times 10^4$ (M <sup>-1</sup> cm <sup>-1</sup> )	<sup>[d]</sup> FWHM nm(cm <sup>-1</sup> )	<sup>[e]</sup> $\lambda_{\text{em}}$ (nm)	<sup>[f]</sup> $\Delta\nu$ nm(cm <sup>-1</sup> )	<sup>[g]</sup> $f$	<sup>[h]</sup> $\Phi_F$
<b>5a</b>	472	6.72	88(4054)	561	89(3361)	1.2354	0.019
<b>5b</b>	479	6.62	86(3843)	583	104(3724)	1.1688	0.118
<b>5c</b>	523	4.84	106(4271)	591	68(2199)	1.039	0.055

<sup>[a]</sup> Analysis was carried out at room temperature (25 °C), <sup>[b]</sup> Absorption maxima (nm), <sup>[c]</sup> Molar extinction coefficient maxima (mol<sup>-1</sup>cm<sup>-1</sup>), <sup>[d]</sup> Full-width half maxima of the absorption band, <sup>[e]</sup> Emission maxima, <sup>[f]</sup> Stokes Shift (nm) cm<sup>-1</sup>, <sup>[g]</sup> Oscillator strength, <sup>[h]</sup> Fluorescence quantum yield.

**Figure 2(b)** displays the emission spectra obtained for the dyes in toluene and corresponding data are provided in **Table 1**. The emission maxima for **5a**, **5b**, and **5c** are 561, 583 and 591 nm respectively. Thus, the emission maxima of the dyes in toluene followed a similar trend to that observed for the absorption spectra. The rigid planar framework and ICT nature of **5c** are reflected in the largely red shifted emission spectrum compared to the other dyes (73, 74). For **5a-c**, the Stokes shift observed are 3361, 3724 and 2199 cm<sup>-1</sup> respectively and are in order **5b** > **5a** > **5c**. Planarity and steric hindrance in the push-pull system plays a

vital role in amplifying the Stokes shift (75). In the ground state, these effects twist the substituent out of the core plane of the fluorophore, forcing the substituent to undergo rotation in the excited state resulting in geometry relaxation. While the substituent rotates in the excited state, a strong interaction between the substituent and the adjoining atoms results in large amount of torsional twist, which is transformed into the Stokes shift. As mentioned above, **5a** and **5b** with freely rotating *N*-alkyl/aryl donors affect the planarity of the system, while **5c** with a julolidine group as a rigid donor induces planarity in the push-pull system. So, we observe here that the absorption and emission bands are in order **5c** > **5b** > **5a**, while the Stokes shifts follow the order **5b** > **5a** > **5c**. The largest Stokes shift is possessed by **5b** in the series, which probably undergoes significant structural reorganization in the excited state due to ICT from D<sub>2</sub> donor to dicyano vinylene unit. (76)

Further, a solvatochromic study was accomplished with solvents of varying polarities so as to perceive the interaction of dyes with solvent both in the ground and excited states. **Figure S1** displays the changes observed in the emission and absorption spectra of the dyes because of the polar environment provided by the solvent. Among the dyes, **5b** displays a solvent insensitive absorption spectra which undoubtedly indicates that the ground state of **5b** is nonpolar in nature and displays insignificant solvent selective association/interaction. A moderate absorption solvatochromism was observed for **5a** and **5c**. Conversely, the emission maxima of the dyes gradually increase on increasing the solvent polarity and hence show positive solvatochromism (see **Figure S1**). This indicates that the dyes are selectively stabilized in an excited state by polar solvents as a result of improved polarization, which is a common phenomenon in dyes substituted with an amino group.(77) In the polar environment, the bathochromically shifted emission spectra of the dyes are as a result of following two aspects, (i) structural reorganization and/or (ii) stabilization in polar solvents due to photoinduced ICT. Comparing the Stokes shifts in nonpolar (toluene) and a polar solvent

(DMSO) further confirms this for the synthesized dyes. For **5a-c**, the calculated shift in emission ( $\Delta\lambda$ ) between the solvents ( $\lambda_{\text{DMSO}}-\lambda_{\text{TOL}}$ ) lie in the range of 55-81 nm and follows the order **5b** (81 nm) > **5a** (62 nm) > **5c** (55 nm). Fluorescence quantum yields ( $\Phi_{\text{F}}$ ) were calculated in different solvents using the reference standard Rhodanine 6G. The  $\Phi_{\text{F}}$  decreased with the increase in the polarity of the solvent indicating that non-radiative relaxation pathway is more preferred in polar solvents than in non-polar solvents. Large Stokes shift and decreased quantum yield in the polar environment cannot originate from geometry relaxation alone, ICT may be responsible for low quantum yields.(78, 79) More drastic effects for **5c** support the above hypothesis where planarization may smoothen CT between julolidine and dicyanovinylene. Furthermore, we compared the reported analogue **1** with this work, as seen from the **Table 4**, substituting different donors at the opposite end resulted in the enhanced optical properties of these dyes. On comparing **1** with **5b** which differs only in the substituent at D<sub>1</sub> position, the absorption displays a small blue shift of 4-8 nm while, in emission a red shift of ~10 nm was observed (**Table 4**). However, in case of **5c**, with rigid donor the effect on the photophysical properties was found to be significant. Thus, keeping the rotor/donor fixed and varying the D<sub>2</sub> with different *N*-substituents enhances the CT characteristic in these dyes thereby giving bathochromically shifted behaviour in absorption and emission.

### Solvent polarity plots and dipole moment

The influence of polar environment of the solvents on the optical properties of the dyes in the ground and excited states was further confirmed by the relationship of emission maxima intensities ( $\lambda_{\text{max}}^{\text{em}}$ ) in cm<sup>-1</sup> with the orientation polarizability ( $\Delta f$ ) of the molecule using Weller (80) and Rettig (81, 82) plots. The Weller and Rettig plots for the dyes are shown in **Figure 3**, which displays a stronger correlations, indicating that stabilization of the excited state is governed by general dye–solvent interactions. For **5a**, **5b**, and **5c** the regression coefficient

obtained from the Weller's plot are 0.88, 0.93, and 0.91 respectively whereas, from the Rettig's plot, they are 0.95, 0.96, and 0.97 respectively. The linear relationship obtained for the dyes over the entire solvent range with the regression coefficient values adjacent to unity, indicates a CT excited state for these dyes.

<FIGURE 3>

The concept arising from the dielectric polarization (83) can be used to express the solvent polarity dependent emission property, which indicates that the spectral differences of the emission upon increasing the solvent polarity are influenced by the change in permanent dipole moments between ground ( $\mu_g$ ) and excited ( $\mu_e$ ) states. The difference in dipole moment between the ground and excited states i.e.  $\Delta\mu = (\mu_e - \mu_g)$  for the dyes were evaluated using the equations (S7) and (S8) shown in the supporting information and are listed in **Table S2**.

Onsager radii ( $a_o$ ) an essential parameter required to solve the above equations were evaluated using B3LYP/6-311++G(d,p) level of theory and are listed in **Table S3**. The  $\Delta\mu$  for **5a-c** was found to be in the range of 3-14 Debye (see **Table S2**). Dye **5b** (8.67 Debye) showed the largest values of  $\Delta\mu$  as compared to **5a** (3.82 Debye) and **5c** (4.22 Debye). This is due to the triphenylamine units at the opposite ends of the  $\pi$ -conjugated framework in **5b** which results in large  $\Delta\mu$ . The rotating phenyl substituents of triphenylamine in **5b** is attached to the central nitrogen atom through a single bond. The rotation of these phenyl rings during the geometry relaxation of the excited state can be explained by two opposing effects (i) the steric hindrance, which forces the phenyl substituent to twist out of the main plane of the fluorophore; (ii) the resonance effect, which provides an inclination to align with the molecular plane to accomplish an improved electron delocalization. In other words, larger perturbation in the molecular structure of **5b** due to its free rotating phenyl rings in both the donors and acceptor results in a vibronically disconcerted structure (75). Thus, the CT characteristic in **5a-c** follows the order as **5b** > **5c** > **5a** (see **Table S2**). Hence, considerable

ICT in **5a-c** is supported by the major difference in dipole moment from the ground to excited state.

Furthermore, the ratio of excited to ground state dipole moment ( $\mu_e/\mu_g$ ) was calculated using the Bilot-Kawshi (84, 85), Bakshiev (86) and Liptay (87) plots and the values obtained are listed in **Table S4**. For **5a-c**, this ratio was found to be higher than unity in each case which clearly rationalizes that the excited state is more polar than the ground state accounting for CT in the excited state in the dyes (see **Table S4**). The  $\mu_e/\mu_g$  obtained by the above mentioned plots follows the same order as the order of  $\Delta\mu$  as **5b** > **5c** > **5a**. Moreover, the dyes with larger values of  $\Delta\mu$  are known to have potentially large non-linearity and hence **5a-c** were further investigated for the NLO properties.

## DFT Study

### Optimized geometries of **5a-c**

The structural and electronic properties of **5a-c** were studied based on the geometries obtained using DFT computation, employing B3LYP/6-311++G(d,p) level of theory. The optimized ground state geometries of **5a-c** in DMSO are displayed in **Figure 4** whereas the relative bond length and bond angle are tabulated in **Table S5**. The bond lengths between donor nitrogen and the adjacent carbon of aryl group in toluene are **5a** (C40 – N43) = 1.3672, **5b** (C40 – N43) = 1.3978 and **5c** (C40 – N41) = 1.3742 Å whereas, the bond lengths in DMSO are **5a** (C40 – N43) = 1.3656, **5b** (C40 – N43) = 1.3976 and **5c** (C40 – N41) = 1.3719. Moreover, as observed from the **Table S5** we see a successive increase and decrease in the bond length of **5a-c** suggesting CT characteristics. Furthermore, in **5a-c** as we move from non-polar to polar solvent the bond shortening observed suggesting CT characteristics to be more prominent in a polar solvent in these dyes. Similarly, other bond lengths between

the secondary D<sub>2</sub> and A groups as seen from the **Table S5** showed bond shortening in DMSO as compared to toluene.

<FIGURE 4>

Further, from **Table S6**, we see that the optimized structures assume a nonplanar arrangement of the auxiliary chromophore at the D<sub>1</sub> donor segment, as depicted in **Figure 4**. The nonplanarity of the D<sub>1</sub> segments in the dyes can be highlighted in terms of the large dihedral angle (37–38°) between the triphenylamine and the dicyanovinylene planes (see **Table S6**). For the dyes, the dihedral angles between the peripheral chromophore (D<sub>2</sub> segment),  $\pi$ -spacer and the dicyanovinylene are in the range of 4 to 6°, which suggests no major twisting in this segment of the conjugation framework. Indicating that the electron donation takes place from the D<sub>2</sub> donor segment rather than the fixed D<sub>1</sub> donor segments, as this segment is more twisted.

### **Electronic transitions, Frontier molecular orbitals (FMO) and Molecular electrostatic potential surface (MEPS)**

Theoretically calculated excitation energies, vertical excitation, oscillator strength and their orbital contributions for **5a-c** estimated using CAM-B3LYP/6-311++G(d,p) are summarized in **Table 2**, whereas with B3LYP/6-311++G(d,p) are listed in **Table S7**. **Figure 5** displays the electronic distribution of the frontier molecular orbitals [highest occupied molecular orbital (HOMO, HOMO-1) and lowest unoccupied molecular orbital (LUMO, LUMO+1)] of the dyes. The HOMOs of **5a-c** are largely delocalized over the D<sub>2</sub> segment and slightly over the dicyano vinylene unit, while the LUMOs are mainly constructed of the molecular orbitals (MO) of the acceptor group i.e. dicyano vinylene. This denotes that there is a substantial CT from the D<sub>2</sub> donor to the acceptor for the visible wavelength absorption with a reasonable

oscillator strength. The LUMO+1 in **5a** and **5c** appears to be solely resided over the D<sub>1</sub> segment, while for **5b** it is scattered over the entire molecule. The HOMO-1 for the dyes are localized over the D<sub>1</sub> segment and slightly over the dicyano vinylene unit. Thus, as observed the prominent absorption in the longer-wavelength region had major contributions from the HOMO→LUMO and slightly from HOMO-1→LUMO electron excitations. The HOMO→LUMO electron excitation would result in migration of the charge from the donor to the while the HOMO-1→LUMO transition indicated a  $\pi$ - $\pi^*$  character (88, 89).

**Table 2.** Computed electronic parameters for the dyes in DCM by TD-DFT (CAM-B3LYP/6-311++G(d,p) level of theory).

Dyes	CAM-B3LYP					
	<sup>[a]</sup> $\lambda_{\text{abs}}$ (nm)	<sup>[b]</sup> $\lambda_{\text{abs}}$ (nm)	<sup>[c]</sup> E (eV)	<sup>[d]</sup> $f$	<sup>[e]</sup> T	<sup>[f]</sup> OC (%)
<b>5a</b>	489	447	2.77	1.27	HOMO → LUMO	92.38
		401	3.09	0.55	HOMO-1 → LUMO	88.08
		253	4.89	0.12	HOMO → LUMO+1	67.23
		263	4.72	0.26	HOMO-1 → LUMO+1	62.72
<b>5b</b>	488	448	2.77	1.39	HOMO → LUMO	85.90
		408	3.04	0.50	HOMO-1 → LUMO	87.35
		268	4.62	0.24	HOMO → LUMO+1	46.82
		267	4.65	0.19	HOMO-1 → LUMO+1	45.91
<b>5c</b>	537	470	2.64	1.30	HOMO → LUMO	93.15
		399	3.11	0.55	HOMO-1 → LUMO	87.62
		264	4.70	0.07	HOMO → LUMO+1	49.29
		263	4.72	0.24	HOMO-1 → LUMO+1	65.91

<sup>[a]</sup> Experimental absorption (nm), <sup>[b]</sup> Theoretical absorption (nm), <sup>[c]</sup> Energy associated with vertical excitations (eV), <sup>[d]</sup> Oscillator strength for theoretical absorption, <sup>[e]</sup> Transitions, <sup>[f]</sup> Orbital contribution for absorption.

Moreover, the electronic energy band gap between HOMO to LUMO levels for **5a-c** were found to be 1.63 eV, 1.65 eV, and 1.56 eV respectively (see **Figure S2**), which further establishes the trend in CT characteristics for **5a-c**. The donor-acceptor substitution pattern determines the energy band gap of the conjugated dyes system. For example, an increase in the donor-acceptor strength of the dyes leads to a decrease in the energy band gap (90). Therefore, an appropriate choice of donor and acceptor groups can successfully lower the energy band gap resulting in efficient CT characteristics within the dyes. The CT characteristics were further succored with the aid of MEPS contour plots for **5a-c** (see **Figure S3**). MEPS plots give a qualitative indication of electrophilic or nucleophilic sites in the dyes by virtue of positive or negative electrostatic potential surfaces (91). From **Figure S3**, the dicyano vinylene segment in the dyes comprises of red color indicating negative electrostatic potential, while the *N*-substituted donor and auxiliary donor/rotor (triphenylamine) segment display blue color indicating positive electrostatic potential surface. From these observations, it is seen that **5a-c** possess a strong electronic transfer from donor to acceptor, resulting in increased ICT character within the dyes. Above observations are suggestive of strong electronic transfer from D-A units indicating an enhanced ICT characteristics within the dyes.

<FIGURE 5>

#### **Natural charges and natural bond order (NBO) analysis from Fock Matrix**

The natural charges on the atoms for **5a-c** were determined using NBO analysis which helps to understand the intramolecular charge distribution and interactions. As previous reports suggest there is no distinct difference in the natural charges obtained at the ground and the excited state (90, 92), so here the natural charges were determined at the ground state only using NBO analysis using the NBO version 3.1 (93) as implemented in the Gaussian 09

program and are summarized in **Table S8**. As expected and found from the result, the nitrogen atom due to its electronegative bear a large negative charge. Further, from **Table S8**, **5a-c** possess alternate negative and positive charges on the atoms within the selected D-A range indicating significant CT characteristics within the dyes. The second order Fock matrix analysis for **5a-c** is constructed so as to investigate the D-A interaction and stabilization energy at B3LYP/6-311++G(d,p) level of theory based on the previous reports. A higher value of  $E^{(2)}$  indicates enhanced D-A interactions resulting in a greater extent of conjugation within the molecule. Increased electron density on C=C bond to anti-bonding orbitals of C=C bond results in such interactions. The  $\pi$ -electrons of C=C bond undergo strong intramolecular hyper conjugative interaction with the C=C anti-bonding orbital in the conjugated system leading to stabilization of molecule. **Tables S9–S11** list the D-A orbital interaction for **5a-c**. For **5a-c** the largest value of  $E^{(2)}$  was found to be 4399.34, 397.24 and 2534.58  $\text{kJ mol}^{-1}$  respectively, whereas the lowest values were found to be 20.18, 26.64 and 20.26  $\text{kJ mol}^{-1}$  respectively. **Table S9** represents D-A orbital interaction for **5a**, in this, the  $\pi$ -electrons of the lone pair (LP) of N1 interacts with the  $\pi^*$  of C2 – C3 increasing the electron density by 0.0241 and leading to stabilization energy of  $\sim 38.38 \text{ kJ/mol}^{-1}$ . This nitrogen was also found to conjugate with  $\pi^*$  of C23 – C24 and C25 – N28 having stabilization energy 20.18 and 39.70  $\text{kJ/mol}^{-1}$ , which is the most energetic interaction with the later one. Further, the  $\pi$ -electrons of C34 – C36 were found to be conjugated with  $\pi^*$  C25 – N28 having stabilization energy 292.67  $\text{kJ/mol}^{-1}$ . It was also found to conjugate with  $\pi^*$  of C52 – C53 having stabilization energy 1440.04  $\text{kJ/mol}^{-1}$  which is the most energetic interaction. Another major interaction was observed with C33 – C34 which interacts with  $\pi^*$  C52 – C53 having stabilization energy 4399.34  $\text{kJ/mol}^{-1}$ . Further, the planarity between the dicyno vinylene acceptor and the secondary D<sub>2</sub> increases the conjugation which suggests delocalization from

the donor to acceptor. These intramolecular interactions from  $\pi$  to  $\pi^*$  results in CT from D<sub>2</sub>-A in **5a-c** subsequently leading to polarization and optical non-linearity in the molecule.

### **Polarizability and hyperpolarizability of 5a-c by spectroscopic and DFT methods.**

Push-pull  $\pi$ -conjugated systems are known to possess excellent non-linear optical properties, which makes them potentially useful in various electronic and optoelectronic devices application (94). In this section, we have investigated the NLO responses of **5a-c** using spectroscopic and DFT methods. The values of polarizability and hyperpolarizability estimated using these methods are compared with with the standard reference NLO material i.e. urea (95). The NLO parameters such as transition dipole moment ( $\mu_{CT}$ ), linear polarizability ( $\alpha_{CT}$ ), first hyperpolarizability ( $\beta_{CT}$ ) and second hyperpolarizability ( $\gamma_{CT}$ ) were calculated using spectroscopic method following the two-level model (96) and are listed in

**Table S12.**  $\mu_{CT}$  of the lowest lying CT excited state for **5a**, **5b**, and **5c** determined using the solvatochromic method are found to be 12.59, 12.17, and 9.82 Debye respectively in DCM. Assuming that the direction of the CT in the dyes coincides with the molecular axis,  $\alpha_{CT}$  were calculated by the equation as described in the literature (96, 97). The solvatochromically derived  $\alpha_{CT}$  values gradually increased with the increase in the solvent polarity for all the dyes. **5a** ( $60-97 \times 10^{-24}$  e.s.u.) exhibits slightly higher values of  $\alpha_{CT}$  compared to **5b** ( $58-78 \times 10^{-24}$  e.s.u.) and **5c** ( $53-8 \times 10^{-24}$  e.s.u.) by the solvatochromic method.

The solvent dependent  $\beta_{CT}$  were determined using the Ouder equation, based on the two-level microscopic model (98, 99). As this model is based on several assumptions, it allows only an approximate estimate of the dominant tensor of total hyperpolarizability along the direction of charge transfer, which is the major contributor to the total hyperpolarizability. However, it is an inexpensive method that gives an insight into the NLO properties of a molecule. The  $\beta_{CT}$  values for **5a**, **5b**, and **5c** are in the range 70-120, 144-190, and 87-124 x

$10^{-30}$  e.s.u. respectively, and highly solvent dependent. **5b** with triphenylamine as both the donors displays higher values of first order hyperpolarizability by the solvatochromic method. A three-level model was used to determine  $\gamma_{CT}$  at the molecular level, arising as a result of electronic polarization in the non-resonant region (100–104). The second order hyperpolarizability regarded as the ‘solvatochromic descriptor’ for the dyes are in the range 139-467, 44-133, and 89-303  $\times 10^{-36}$  e.s.u. respectively. Thus, from the above observation,  $\gamma_{CT}$  values for **5a** and **5c** are found to be higher than that of **5b** by the solvatochromic method.

**Table 3.** Computationally measured first order hyperpolarizability of **5a-c** using various functionals with 6-311++G(d,p) basis set.

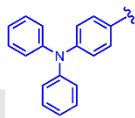
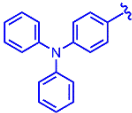
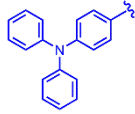
First order hyperpolarizability ( $\beta_0$ )							
(x $10^{-30}$ e.s.u.)							
Dyes	Solvent	B3LYP	BHLLYP	CAM-B3LYP	$\omega$ B97	$\omega$ B97X	$\omega$ B97XD
<b>5a</b>	DCM	402	299	331	294	300	317
	DMSO	481	364	406	362	370	390
<b>5b</b>	DCM	659	368	387	269	289	342
	DMSO	779	426	449	310	333	396
<b>5c</b>	DCM	437	384	427	397	402	415
	DMSO	524	476	533	505	509	522

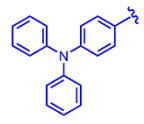
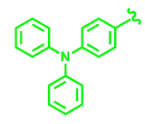
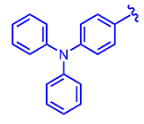
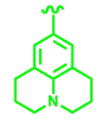
Further, the theoretical NLO parameters for **5a-c** such as Onsager radii ( $a_0$ ), static dipole moment ( $\mu_0$ ), mean polarizability ( $\alpha_0$ ), static first order hyperpolarizability ( $\beta_0$ ) and second order hyperpolarizability ( $\gamma_0$ ) were calculated using two global hybrid functionals (B3LYP and BHLLYP) and four range-separated hybrid functionals (CAM-B3LYP,  $\omega$ B97,  $\omega$ B97X,  $\omega$ B97XD) so as to compare the results obtained by the global hybrid (GH) and range-separated hybrid (RSH) functionals (see **Table 3** and **S13-16**). B3LYP and BHLLYP a GH functional have a constant percentage of HF exchange i.e. 20 and 50% respectively,

whereas CAM-B3LYP (19-65%),  $\omega$ B97 (0-100%),  $\omega$ B97 (15.77-100%), and  $\omega$ B97 (22.2-100%) an improved range separated hybrid functional known for their better performance than that of hybrid functional. These NLO parameters were calculated theoretically and experimentally based on the theory described in our previous reports (105, 106). The basis set used was the standard triple zeta basis set as 6-311++G(d,p). Here, we have compared the NLO parameters obtained using GH and RSH functionals, the results obtained are in good agreement with both the functionals used. For **5a-c**, the calculated values of polarizability and hyperpolarizability are found to be solvent dependent. Further, altering the transition dipole moment results in tailored NLO responses for the particular dye (107, 108). The molecular hyperpolarizability for **5a-c** is found to increase with the increase in solvent polarity (**Table 3**). Moreover, varying donor and acceptor strength accounts for the altered polarizability and hyperpolarizability values of **5a-c**. For **5a-c**, the theoretically derived values of  $\alpha$ ,  $\beta$ , and  $\gamma$  are in the range  $100-118 \times 10^{-24}$  e.s.u.,  $299-476 \times 10^{-30}$  e.s.u., and  $1,630-2,989 \times 10^{-36}$  e.s.u. respectively with BHHLYP functional, while with  $\omega$ B97XD these values are in the range  $100-119 \times 10^{-24}$  e.s.u.,  $317-522 \times 10^{-30}$  e.s.u., and  $1,558-2,299 \times 10^{-36}$  e.s.u. respectively (see **Table 3, S14 and 16**). These values are found to be larger compared with that of urea ( $\alpha_{\text{urea}} = 6.2 \times 10^{-24}$  e.s.u.,  $\beta_{\text{urea}} = 0.31 \times 10^{-30}$  e.s.u.,  $\gamma_{\text{urea}} = 4.46 \times 10^{-36}$  e.s.u.), suggesting enhanced NLO response in **5a-c**. The values of polarizability and hyperpolarizability obtained with BHHLYP functional was found to be comparable with the RSH functionals. Further, on comparing the  $\beta_0$  values with that of known analogue **1** the dyes (**5a-c**) showed higher values (**Table 4**). This is due to stronger D-A strength,  $\pi$ -conjugation length as well as the non-centrosymmetry resulting from triphenylamine group (fixed rotor/donor) which increases the non-linearity in **5a-c** leading to improved NLO properties compared to reported analogue **1**. Thus, the optical and NLO properties of **5a-c** were greatly influenced by substituting various donor groups at the D<sub>2</sub> position and keeping the primary rotor/ donor fixed.

Theoretical limits for the hyperpolarizability values were calculated using the equations (S3) and (S4) based on the limiting theory proposed by Kuzyk (109) described in the supporting information, and the limiting values are summarized in **Table S17**. The  $\gamma$  values have two fundamental limits - a negative centrosymmetric limit and the positive limit for an asymmetric NLO molecule. From the equation (S3) and (S4) the optical limiting values obtained for  $\beta$  and  $\gamma$  were compared with the values obtained from the solvatochromic shift and theoretical methods for **5a-c**. From the results, it is observed that the values of  $\beta$  and  $\gamma$  lie within the estimated limiting values.

**Table 4.** Comparison of reported analogue **1** with the **5a-c**.

Donor/Rotor	Donor	<sup>[a]</sup> $\lambda_{\text{abs}}$		<sup>[b]</sup> $\lambda_{\text{emi}}$		<sup>[c]</sup> $\beta_0$ (x 10 <sup>-30</sup> e.s.u.)	Reference
		(nm)		(nm)			
		Toluene	DMF	Toluene	DMF		
	--	439	ND	449	ND	125 (Toluene)	(110)
		487	490	574	654	196 (gas)	(59)
		472	499	561	623	331 (DCM)	This Work

		479	486	583	664	387 (DCM)	This Work
		523	557	591	646	427 (DCM)	This Work

<sup>[a]</sup> Experimental absorption (nm), <sup>[b]</sup> Experimental emission (nm), <sup>[c]</sup> First order hyperpolarizability.

### Bond length alternation (BLA) and Bond order alternation (BOA): Correlation with NLO properties.

BLA and BOA are regarded as the geometric and electronic parameters governed by the D-A strength, length of  $\pi$ -conjugation and the surrounding media. The BLA and BOA for **5a-c** were calculated from the optimized geometry at the ground state. These parameters for all the dyes were correlated to  $\beta_0$  values **Figure 6** and the results are summarized in **Table S18**.

**Figure 6** shows a linear relation of  $\beta_0$  values with those of BLA and BOA values. The BLA values are found to decrease in the order **5b** > **5a** > **5c**, while BOA values decrease in the order **5b** > **5c** > **5a**. As seen from the **Table S18**, the BLA and BOA values are approaching towards the zero suggesting a high degree of polarization in the synthesized dyes. Greater the polarization for the dyes higher is the  $\mu$ ,  $\alpha_0$  and  $\beta_0$  values leading to decreased BLA and BOA (92). Moreover, the magnitude of  $\mu$ ,  $\alpha_0$ , and  $\beta_0$  increases with the increase in the D-A strength and the length of  $\pi$ -conjugation as observed for **5c**. From the above implications, it is observed that the trends obtained in  $\mu$ ,  $\alpha_0$  and  $\beta_0$  are found to be in good agreement with observed trends of BLA and BOA.

<FIGURE 6>

## Z-scan

The third order non-linear optical properties of the dyes were analyzed using the Z-scan analysis (111). Wavelength dependent macroscopic parameter viz. the magnitude of non-linear absorption coefficient ( $\beta$ ), the magnitude of non-linear refraction ( $n_2$ ) and third order non-linear susceptibility ( $\chi^{(3)}$ ) were estimated from the Z-scan analysis. The macroscopic parameter like third order non-linear susceptibility ( $\chi^{(3)}$ ) were determined using the values of  $\beta$  and  $n_2$ . In the Z-scan analysis, the  $\beta$  was evaluated from the open aperture (OA) Z-scan measurements, while  $n_2$  was determined by the closed aperture (CA) Z-scan measurement (111, 112).

The magnitude of non-linear absorption coefficient ( $\beta$ ) and the magnitude of non-linear refraction ( $n_2$ ) for the dyes was calculated using measurements of closed (CA) and open aperture (OA) of Z-scan techniques in solvents such as acetone, ethanol, and DMSO at  $0.3 \times 10^{-3}$  M concentration. The normalized open aperture and close aperture Z-scan curves for the dyes in DMSO solvent are shown in **Figure 7** and for remaining solvents in **Figure S4-S6** in ESI. OA curves of the dyes in DMSO shows a saturable absorption thereby displaying a negative type of absorption non-linearity resulting in negative  $\beta$  values. However, the OA curves of **5a** (in acetone) and **5b** (in acetone and ethanol) shows a reverse saturable absorption (see **Figure S4** and **S5**) displaying a positive type of absorption non-linearity resulting in positive values of  $\beta$  (**Table 5**). Further, closed aperture z-scan experiment was performed to measure the non-linear index of refraction ( $n_2$ ). In this process of non-linear refraction, the refractive index of the medium fluctuates as a result of high intensity laser beam. Moreover, the real part of  $\chi^{(3)}$  can be obtained by evaluating the  $n_2$  values. As can be seen from the **Figure 7**, the plot of closed aperture z-scan analysis for the dyes exhibit the prefocal transmittance minimum (valley) followed by the post focal transmittance maximum (peak) type of behaviour. This alternate prefocal and post focal

transmittance can be attributed to the characteristic behaviour of chromophores with the positive non-linear refractive index as a result of self-focusing. Hence, the dyes possess positive  $n_2$  values (**Table 5**. Division of closed aperture data by open aperture data gives the pure non-linear refraction curves.

<FIGURE 7>

The values of  $\beta$ ,  $n_2$ , and  $\chi^{(3)}$  calculated are listed in **Table 5**. The  $\beta$  values contribute to the imaginary part of the third order non-linear susceptibility ( $Im \chi^{(3)}$ ) and should display minimum values whereas  $n_2$  values pay to the real part of ( $Re \chi^{(3)}$ ) and value should be high in order to have practical applications. At the same time, the non-linear absorption should be as small as possible. Consequently, these two criteria collectively lead to higher values of  $\chi^{(3)}$  for the synthesized dyes. From **Table 5** it is seen that the values of  $Re \chi^{(3)}$  are found to be larger as compared to the  $Im \chi^{(3)}$  which collectively produces the large values of  $\chi^{(3)}$  for all the dyes. Comparatively, **5b** exhibits a higher values of  $\chi^{(3)}$  in the range  $2.94 - 6.10 \times 10^{-13}$  e.s.u., whereas **5a** and **5c** show lower values,  $1.71 - 4.63 \times 10^{-13}$  e.s.u in studied solvents with **5b** showing the highest value in ethanol ( $6.10 \times 10^{-13}$  e.s.u).

**Table 5.** Third-order non-linear optical parameters of dyes **5a-c**.

Dyes	Solvent	<sup>[a]</sup> $\beta$ ( $\times 10^{-12}$ ) (m/W)	<sup>[b]</sup> $n_2$ ( $\times 10^{-19}$ ) (m <sup>2</sup> /W)	<sup>[c]</sup> $Re \chi^{(3)}$ ( $\times 10^{-13}$ ) (e.s.u.)	<sup>[d]</sup> $Im \chi^{(3)}$ ( $\times 10^{-13}$ ) (e.s.u.)	<sup>[e]</sup> $\chi^{(3)}$ ( $\times 10^{-13}$ ) (e.s.u.)
<b>5a</b>	Acetone	8.0206	2.8271	1.0932	1.3137	1.7091
	Ethanol	-4.6908	10.9237	4.5569	-0.8288	4.6317
	DMSO	-7.3464	9.9227	3.9605	-1.2420	4.1507
<b>5b</b>	Acetone	12.3288	8.2781	3.2260	2.0351	3.8143
	Ethanol	30.7582	0.1144	0.0536	6.0990	6.0992

	DMSO	-7.6930	6.1407	2.5981	1.3787	2.9413
	Acetone	-8.7152	3.7832	1.2770	-1.2461	1.7842
<b>5c</b>	Ethanol	-6.8325	8.1432	3.3843	-0.9399	3.5124
	DMSO	-6.7968	3.7808	1.4717	-1.1206	1.8498

### Optical limiting measurements

The characteristic optical limiting curve as a function of incident fluence varying from 0 Jcm<sup>-2</sup> to 40 Jcm<sup>-2</sup> for **5a** and **5b** in two solvents is displayed in **Figure 8**. At low incident fluence, the output changes linearly i.e. the linear transmission obeyed Beer's law,  $I = I_0 e^{-\alpha L}$  where,  $I$  is output intensity,  $I_0$  is input intensity,  $\alpha$  is absorption coefficient and  $L$  is the thickness of the sample. Furthermore, it is observed that (**Figure 8**), as the input intensity increases, the linear transmission starts to deviate from linearity and one can observe the optical limiting curve. The deviation from the linearity is observed both the dyes. The optical limiting curve can be plotted as input fluence vs. transmittance (**Figure 9**). Optical limiting values for **5a** and **5b** in acetone was found to be 17.20 and 9.55 Jcm<sup>-2</sup> respectively, whereas in ethanol it was 6.43 Jcm<sup>-2</sup> for **5b**.

<FIGURE 8>

<FIGURE 9>

### Laser damage threshold study

Important information on the maximum permissible laser power which an NLO crystal can withstand without getting damaged are obtained through laser damage study (113). Several factors like specific heat, thermal conductivity, optical absorption, etc. govern the laser

damage threshold of the NLO crystal. The following expression was used to calculate the surface damage threshold of the crystal:

$$LDT(\lambda_2\tau_2) \sim LDT(\lambda_1\tau_1) \left(\frac{\lambda_2}{\lambda_1}\right) \sqrt{\frac{\tau_2}{\tau_1}}$$

where,

$\tau_1$  is the laser pulse length and  $\lambda_1$  is the laser wavelength for the given LDT and

$\tau_2$  is the laser pulse length and  $\lambda_2$  is the laser wavelength with unknown LDT.

$$\text{power density } (P_d) = \frac{E}{\pi r^2 t}$$

where

E is the energy in (mJ),

t is the pulse width (ns) and

r is the radius of the beam spot in mm.

Laser damage threshold values for **5a**, **5b**, and **5c** were found to be 4.60, 4.37, and 3.37 GW cm<sup>-2</sup> respectively. The values of laser damage threshold for the dyes when compared to the reported value of the standard inorganic material,  $\beta$ -BBO crystals at same specification (114) were found to be several times higher than.

### Two photon absorption (2PA) cross section from the spectroscopic method

The 2PA cross-section for **5a-c** are calculated using the equation (S7) described in the supporting information for the two-level model and results are summarized in **Table 6**. The 2PA cross-section values obtained in toluene for **5a**, **5b**, and **5c** are 47.51, 250.63, and 44.00 GM respectively. Similarly, these values obtained in DMSO for **5a**, **5b**, and **5c** are 68.91, 299.56, and 65.69 GM respectively. **5a** and **5c** showed the lowest values of the 2PA cross-section whereas, **5b** showed the largest value, as a result of efficient CT character within the

dye. Interestingly, the 2PA cross-section for **5a-c** was found to follow the same trend as of Stokes shift in the order **5b** > **5a** > **5c** (115). Thus, increasing the  $\pi$ -conjugation with enforced co-planarity leads to higher 2PA cross-section. From the above results, we observed that the styryl dyes with greater values of dipole moment ( $\Delta\mu_{eg}$ ), molar extinction coefficient ( $\epsilon_{max}$ ) and larger 1PA values showed higher 2PA cross-section. The values for dipole moment difference and 2PA cross-section obtained by the solvatochromic method are overemphasized, as we have considered several assumptions in the two level model. However, to understand the 2PA cross-section trend of the styryl dyes in cost effective way this solvatochromic two level model serves as a primary tool.

**Table 6.** Two photon cross section in GM for **5a-c** in different solvents using the solvatochromic method.

Solvents	$\sigma_{2PA}$ (GM)		
	<b>5a</b>	<b>5b</b>	<b>5c</b>
Toluene	47.51	250.63	44.00
DCM	46.16	245.71	48.35
EtOAc	52.81	288.54	36.46
Acetone	51.03	266.49	48.93
DMF	58.76	200.28	57.54
DMSO	68.91	299.56	65.69

## Conclusion

In summary, three triphenylamine (fixed rotor/ donor) based D- $\pi$ -A- $\pi$ -D hybrid dyes (**5a-c**) with varying *N*-substituted secondary donors and dicyano vinylene as an acceptor were designed and successfully synthesized. The dyes displayed positive solvatochromism

behavior from non-polar (toluene) to polar (DMSO) environment, more preferably emission solvatochromism (55-81 nm) which is due to the charge transfer from D<sub>2</sub> donor to the acceptor. The dyes **5a-c** showed reasonable sign of CT characteristics as observed by the solvent polarity plots drawn on the basis of Weller and Rettig models. The molecular geometries of the synthesized dyes were optimized and theoretically investigated using DFT computations to gain significant insight into the fundamental structural and electronic properties of **5a-c**. TD-DFT computations were also performed to establish the correlations between electronic structure and photophysical properties of the dyes. The polarizability and hyperpolarizability values for **5a-c** were estimated using spectroscopic, theoretical and Z-scan methods and were found to be superior compared to that of reference material, making them suitable for the non-linear optical materials. The values obtained from Z-scan for non-linear absorption coefficient ( $\beta$ ) in DMSO are -7.34, -7.69, and -6.80 x 10<sup>-12</sup> (m/W) respectively and for third order non-linear susceptibility ( $\chi^{(3)}$ ) are 4.15, 2.94, and 1.85 x 10<sup>-13</sup> (e.s.u.) respectively. The two-photon absorption cross section values obtained for **5b** (251-300 GM) were found to be larger than **5a** and **5c**.

*Acknowledgment*-The author is thankful to the University Grant Commission (U.G.C.), New Delhi, India for the award of Junior and Senior Research Fellowship.

### Supporting Information

Additional supporting information may be found online in the Supporting Information section at the end of the article.

**Figure S1.** Normalized absorption and emission spectra of the dyes **5a-5d** in different solvents.

**Figure S2.** HOMO-LUMO energy level diagram of dyes **5a-c**.

**Figure S3.** Molecular electrostatic potential (MEP) surface of the dyes **5a-c**.

**Figure S4-S6.** Normalized closed aperture and closed aperture Z-scan curves for dyes **5a-c** in different solvents.

**Table S1.** Photophysical parameters of **5a-c** in solvents of different polarities.

**Table S2.** Difference in the dipole moments of **5a-c**.

**Table S3.** Onsager radii ( $a_0$ ) in Å for the dyes **5a-c**.

**Table S4.** Ratio of dipole moment between ground and excited state of **5a-c** by various method.

**Table S5.** Selected bond length (Å) for **5a-c** in toluene and DMSO.

**Table S6.** Selected dihedral angle (°) for **5a-c**.

**Table S7.** Computed electronic parameters for the dyes in DCM by TD-DFT (B3LYP/6-311++G(d,p) level of theory).

**Table S8.** Natural charges on the selected atoms within dyes **5a-c** in the ground state ( $S_0$ ).

**Table S9-S11.** Second order perturbation theory analysis of the Fock matrix in NBO basis for **5a-c**.

**Table S12-S16.** Solvatochromic and theoretically calculated linear and non-linear optical properties of dyes **5a-c**.

**Table S17.** Comparison of spectroscopic and theoretical values with the limiting values of hyperpolarizability for **5a-c**.

**Table S18.** BLA and BOA index of **5a-c** at the ground state ( $S_0$ ).

And  $^1\text{H}$  and  $^{13}\text{C}$  NMR spectra of the dyes **5a-c**.

## References

1. Jiao, G. S., Thoresen, L. H. and Burgess, K. (2003) Fluorescent, Through-Bond Energy Transfer Cassettes for Labeling Multiple Biological Molecules in One Experiment. *J. Am. Chem. Soc.* **125**, 14668–14669. <https://doi.org/10.1021/ja037193l>.
2. Lai, R. Y., Fabrizio, E. F., Lu, L., Jenekhe, S. a, Bard, A. J., January, R. V, Re, V., Recci, M. and June, V. (2001) Synthesis, Cyclic Voltammetric Studies, and Electrogenerated Chemiluminescence of a New DonorsAcceptor Molecule: 3,7-[Bis[4-phenyl-2-quinoly]]-10-methylphenothiazine. *J. Am. Chem. Soc.* **123**, 9112–9118. <https://doi.org/10.1021/ja036600q>.
3. Albota, M. (1998) Design of Organic Molecules with Large Two-Photon Absorption Cross Sections. *Science* (80-. ). **281**, 1653–1656. <https://doi.org/10.1126/science.281.5383.1653>.
4. Staub, K., Levina, G. A., Barlow, S., Kowalczyk, T. C., Lackritz, H. S., Barzoukas, M., Fort, A. and Marder, S. R. (2003) Synthesis and stability studies of conformationally locked 4-(diarylamino)aryl- and 4-(dialkylamino)phenyl-substituted second-order nonlinear optical polyene chromophores. *J. Mater. Chem.* **13**, 825–833. <https://doi.org/10.1039/b208024a>.
5. Zhang, X. H., Chen, B. J., Lin, X. Q., Wong, O. Y., Lee, C. S., Kwong, H. L., Lee, S. T. and Wu, S. K. (2001) Article A New Family of Red Dopants Based on Chromene-Containing Compounds for Organic Electroluminescent Devices A New Family of Red Dopants Based on Chromene-Containing Compounds for Organic Electroluminescent Devices. *Chem. Mater.* **13**, 1565–1569. <https://doi.org/10.1021/cm0008664>.
6. Tao, X. T., Miyata, S., Sasabe, H., Zhang, G. J., Wada, T. and Jiang, M. H. (2001) Efficient organic red electroluminescent device with narrow emission peak. *Appl. Phys. Lett.* **78**, 279–281. <https://doi.org/10.1063/1.1341226>.
7. Law, K. Y. (1993) Organic photoconductive materials: recent trends and developments. *Chem. Rev.* **93**, 449–486. <https://doi.org/10.1021/cr00017a020>.
8. Lambert, C., Schelter, J., Fiebig, T., Mank, D. and Trifonov, A. (2005) Photoinduced charge transfer processes along triarylamine redox cascades. *J. Am. Chem. Soc.* **127**, 10600–10610. <https://doi.org/10.1021/ja0511570>.
9. Antonietta Loi, M., Denk, P., Hoppe, H., Neugebauer, H., Winder, C., Meissner, D., Brabec, C., Serdar Sariciftci, N., Gouloumis, A., Vázquez, P. and Torres, T. (2003) Long-lived photoinduced charge separation for solar cell applications in phthalocyanine–fulleropyrrolidine dyad thin filmsElectronic supplementary information (ESI) available: plots of the refractive index, extinction coefficient and dielectric function o. *J. Mater. Chem.* **13**, 700–704. <https://doi.org/10.1039/b212621d>.
10. Wong, M. S., Li, Z. H., Tao, Y. and Iorio, M. D. (2003) Synthesis and Functional

Properties of Donor - Acceptor  $\pi$  -Conjugated Oligomers. *Chem. Mater.* **15**, 1198–1203.

11. Furumi, S. and Tamaoki, N. (2010) Glass-forming cholesteric liquid crystal oligomers for new tunable solid-state laser. *Adv. Mater.* **22**, 886–891.

<https://doi.org/10.1002/adma.200902552>.

12. Mor, G. K., Basham, J., Paulose, M., Kim, S., Varghese, O. K., Vaish, A., Yoriya, S. and Grimes, C. A. (2010) High-efficiency forster resonance energy transfer in solid-state dye sensitized solar cells. *Nano Lett.* **10**, 2387–2394. <https://doi.org/10.1021/nl100415q>.

13. Song, Y., Di, C., Yang, X., Li, S., Xu, W., Liu, Y., Yang, L., Shuai, Z., Zhang, D. and Zhu, D. (2006) A Cyclic Triphenylamine Dimer for Organic Field-Effect Transistors with High Performance. *J. Am. Chem. Soc.* **128**, 15940–15941.

14. Tsai, J., Chueh, C., Lai, M., Chen, W., Ko, B., Ting, C. and Wang, C. (2009) Synthesis of New Indolocarbazole-Acceptor Alternating Conjugated Copolymers and Their Applications to Thin Film Transistors and Photovoltaic Cells Synthesis of New Indolocarbazole-Acceptor Alternating Conjugated Copolymers and Their Applications to Thin F. *Macromolecules* **42**, 1897–1905. <https://doi.org/10.1021/ma802720n>.

15. Wang, C., Dong, H., Hu, W., Liu, Y. and Zhu, D. (2012) Semiconducting  $\pi$ -Conjugated Systems in Field-Effect Transistors: a material odyssey of organic electronics. *Chem. Rev.* **2208**. <https://doi.org/10.1021/cr100380z>.

16. Bureš, F. (2014) Fundamental aspects of property tuning in push–pull molecules. *RSC Adv.* **4**, 58826–58851. <https://doi.org/10.1039/C4RA11264D>.

17. Janiga, A., Bednarska, D., Thorsted, B., Brewer, J. and Gryko, D. T. (2014) Quadrupolar, emission-tunable  $\pi$ -expanded 1,4-dihydropyrrolo[3,2-b]pyrroles – synthesis and optical properties. *Org. Biomol. Chem.* **12**, 2874–2881. <https://doi.org/10.1039/C4OB00143E>.

18. Hrobárik, P., Hrobáriková, V., Semak, V., Kasák, P., Rakovský, E., Polyzos, I., Fakis, M. and Persephonis, P. (2014) Quadrupolar benzobisthiazole-cored arylamines as highly efficient two-photon absorbing fluorophores. *Org. Lett.* **16**, 6358–6361. <https://doi.org/10.1021/ol503137p>.

19. Zou, L., Liu, Z., Yan, X., Liu, Y., Fu, Y., Liu, J., Huang, Z., Chen, X. and Qin, J. (2009) Star-shaped D- $\pi$ -A molecules containing a 2,4,6-tri(thiophen-2-yl)-1,3,5- triazine unit: Synthesis and two-photon absorption properties. *European J. Org. Chem.* 5587–5593. <https://doi.org/10.1002/ejoc.200900641>.

20. Huang, H.-F., Xu, S.-H., He, Y.-B., Zhu, C.-C., Fan, H.-L., Zhou, X.-H., Gao, X.-C. and Dai, Y.-F. (2013) Synthesis and characterization of highly stable and efficient star-molecules. *Dye. Pigment.* **96**, 705–713. <https://doi.org/10.1016/j.dyepig.2012.11.014>.

21. Cvejn, D., Michail, E., Polyzos, I., Almonasy, N., Pytela, O., Klikar, M., Mikysek, T., Giannetas, V., Fakis, M. and Bures, F. (2015) Modulation of (non)linear optical properties in tripodal molecules by variation of the peripheral cyano acceptor moieties and the pi-spacer. *J. Mater. Chem. C* **3**, 7345–7355. <https://doi.org/10.1039/c5tc01293g>.

22. Wang, J., Xiao, Q. and Pei, J. (2010) Benzothiadiazole-Based D -  $\pi$  -A -  $\pi$  -D Organic Dyes with Tunable Band Gap : Synthesis and Photophysical Properties. *Org Lett* **12**, 2008–2011.

23. Clifford, J. N., Martínez-Ferrero, E., Viterisi, A. and Palomares, E. (2011) Sensitizer molecular structure-device efficiency relationship in dye sensitized solar cells. *Chem. Soc. Rev.* **40**, 1635–1646. <https://doi.org/10.1039/B920664G>.
24. Li, X., Hu, Y., Sanchez-Molina, I., Zhou, Y., Yu, F., Haque, S. A., Wu, W., Hua, J., Tian, H. and Robertson, N. (2015) Insight into quinoxaline containing D- $\pi$ -A dyes for dye-sensitized solar cells with cobalt and iodine based electrolytes: the effect of  $\pi$ -bridge on the HOMO energy level and photovoltaic performance. *J. Mater. Chem. A* **3**, 21733–21743. <https://doi.org/10.1039/C5TA07254A>.
25. Velusamy, M., Thomas, K. R. J., Lin, J. T., Hsu, Y. C. and Ho, K. C. (2005) Organic dyes incorporating low-band-gap chromophores for dye-sensitized solar cells. *Org. Lett.* **7**, 1899–1902. <https://doi.org/10.1021/ol050417f>.
26. Zhu, W., Wu, Y., Wang, S., Li, W., Li, X., Chen, J., Wang, Z. S. and Tian, H. (2011) Organic D-A- $\pi$ -A solar cell sensitizers with improved stability and spectral response. *Adv. Funct. Mater.* **21**, 756–763. <https://doi.org/10.1002/adfm.201001801>.
27. Li, Y., Guo, Q., Li, Z., Pei, J. and Tian, W. (2010) Solution processable D-A small molecules for bulk-heterojunction solar cells. *Energy Environ. Sci.* **3**, 1427. <https://doi.org/10.1039/c003946b>.
28. Walker, B., Kim, C. and Nguyen, T. Q. (2011) Small molecule solution-processed bulk heterojunction solar cells. *Chem. Mater.* **23**, 470–482. <https://doi.org/10.1021/cm102189g>.
29. Zhang, C. Z., Lu, C., Zhu, J., Lu, G. Y., Wang, X., Shi, Z. W., Liu, F. and Cui, Y. (2006) The second-order nonlinear optical materials with combined nonconjugated D- $\pi$ , -A units. *Chem. Mater.* **18**, 6091–6093. <https://doi.org/10.1021/cm0618042>.
30. Myung Kim, H. and Rae Cho, B. (2009) Two-photon materials with large two-photon cross sections. Structure–property relationship. *Chem. Commun.* 153–164. <https://doi.org/10.1039/B813280A>.
31. Wang, C., Zhang, T. and Lin, W. (2012) Rational synthesis of noncentrosymmetric metal-organic frameworks for second-order nonlinear optics. *Chem. Rev.* **112**, 1084–1104. <https://doi.org/10.1021/cr200252n>.
32. Ekbote, A., Patil, P. S., Maidur, S. R., Chia, T. S. and Quah, C. K. (2017) Structure and nonlinear optical properties of (E)-1-(4-aminophenyl)-3-(3-chlorophenyl) prop-2-en-1-one: A promising new D- $\pi$ -A- $\pi$ -D type chalcone derivative crystal for nonlinear optical devices. *J. Mol. Struct.* **1129**, 239–247. <https://doi.org/10.1016/j.molstruc.2016.09.077>.
33. Ramkumar, V., Anandhi, S., Kannan, P. and Gopalakrishnan, R. (2013) Synthesis, single crystal growth, characterization and comparison of two new enone shifted chalcones and their NLO behaviour. *CrystEngComm* **15**, 2438. <https://doi.org/10.1039/c2ce26185e>.
34. Thomas, K. R. J., Velusamy, M., Lin, J. T., Sun, S.-S., Tao, Y.-T. and Chuen, C.-H. (2004) Energy harvesting star-shaped molecules for electroluminescence applications. *Chem. Comm.* **20**, 2328–2329. <https://doi.org/10.1039/b409800e>.
35. Kanis, D. R., Ratner, M. A. and Marks, T. J. (1994) Design and Construction of Molecular Assemblies with Large Second-Order Optical Nonlinearities. Quantum Chemical Aspects. *Chem. Rev.* **94**, 195–242. <https://doi.org/10.1021/cr00025a007>.

36. Ma, N. N., Yang, G. C., Sun, S. L., Liu, C. G. and Qiu, Y. Q. (2011) Computational study on second-order nonlinear optical (NLO) properties of a novel class of two-dimensional  $\pi$ - and W-shaped sandwich metallocarborane-containing chromophores. *J. Organomet. Chem.* **696**, 2380–2387. <https://doi.org/10.1016/j.jorganchem.2011.03.004>.
37. Yang, M. and Champagne, B. (2003) Large off-diagonal contribution to the second-order optical nonlinearities of  $\Lambda$ -shaped molecules. *J. Phys. Chem. A* **107**, 3942–3951. <https://doi.org/10.1021/jp0272567>.
38. Teimuri-Mofrad, R., Rahimpour, K. and Ghadari, R. (2017) Design, synthesis and characterization of ferrocene based V-shaped chromophores with modified nonlinear effect. *J. Organomet. Chem.* **846**, 397–406. <https://doi.org/10.1016/j.jorganchem.2017.07.023>.
39. Lee, H., An, S.-Y. and Cho, M. (1999) Nonlinear Optical (NLO) Properties of the Octupolar Molecule: Structure–Function Relationships and Solvent Effects. *J. Phys. Chem. B* **103**, 4992–4996. <https://doi.org/10.1021/jp990798c>.
40. Kim, E. and Park, S. B. (2009) Chemistry as a prism: A review of light-emitting materials having tunable emission wavelengths. *Chem. - An Asian J.* **4**, 1646–1658. <https://doi.org/10.1002/asia.200900102>.
41. Jeong, M. Y. and Cho, B. R. (2015) Octupolar molecules for nonlinear optics: From molecular design to crystals and films with large second-harmonic generation. *Chem. Rec.* **15**, 132–142. <https://doi.org/10.1002/tcr.201402013>.
42. Terenziani, F., Painelli, A., Katan, C., Charlot, M. and Blanchard-Desce, M. (2006) Charge instability in quadrupolar chromophores: Symmetry breaking and solvatochromism. *J. Am. Chem. Soc.* **128**, 15742–15755. <https://doi.org/10.1021/ja064521j>.
43. Gauthier, S., Vologdin, N., Achelle, S., Barsella, A., Caro, B. and Robin-Le Guen, F. (2013) Methylenepyran based dipolar and quadrupolar dyes: Synthesis, electrochemical and photochemical properties. *Tetrahedron* **69**, 8392–8399. <https://doi.org/10.1016/j.tet.2013.07.066>.
44. Taniuchi, T., Okada, S. and Nakanishi, H. (2004) Widely tunable terahertz-wave generation in an organic crystal and its spectroscopic application. *J. Appl. Phys.* **95**, 5984–5988. <https://doi.org/10.1063/1.1713045>.
45. Čibová, A., Martinická, A., Magdolen, P., Zahradník, P., Cigáň, M., Uherek, M. and Chorvát, D. (2018) Dicationic and monocationic benzobisthiazolium salts as potential NLO chromophores. *Dye. Pigment.* **149**, 597–611. <https://doi.org/10.1016/J.DYEPIG.2017.11.015>.
46. Schneider, A., Neis, M., Stillhart, M., Ruiz, B., Khan, R. U. A. and Günter, P. (2006) Generation of terahertz pulses through optical rectification in organic DAST crystals: theory and experiment. *J. Opt. Soc. Am. B* **23**, 1822. <https://doi.org/10.1364/JOSAB.23.001822>.
47. Taniuchi, T., Ikeda, S., Okada, S. and Nakanishi, H. (2005) Tunable sub-terahertz wave generation from an organic DAST crystal. *Japanese J. Appl. Physics, Part 2 Lett.* **44**, 1–4. <https://doi.org/10.1143/JJAP.44.L652>.
48. Lee, H. J., Sohn, J., Hwang, J., Park, S. Y., Choi, H. and Cha, M. (2004) Triphenylamine-Cored Bifunctional Organic Molecules for Two-Photon Absorption and Photorefraction. *Chem. Mater.* **16**, 456–465. <https://doi.org/10.1021/cm0343756>.

49. Fang, Z., Zhang, X., Hing Lai, Y. and Liu, B. (2009) Bridged triphenylamine based molecules with large two-photon absorption cross sections in organic and aqueous media. *Chem. Commun. (Camb)*. 920–922. <https://doi.org/10.1039/b812649f>.
50. Yang, W. J., Kim, D. Y., Jeong, M. Y., Kim, H. M., Lee, Y. K., Fang, X., Jeon, S. J. and Cho, B. R. (2005) Two-photon absorption properties of 2,6-bis(styryl)anthracene derivatives: Effects of donor-acceptor substituents and the  $\pi$  center. *Chem. - A Eur. J.* **11**, 4191–4198. <https://doi.org/10.1002/chem.200401134>.
51. Yang, M., Xu, D., Xi, W., Wang, L., Zheng, J., Huang, J., Zhang, J., Zhou, H., Wu, J. and Tian, Y. (2013) Aggregation-Induced Fluorescence Behavior of Triphenylamine- Based Schiff Bases: The Combined Effect of Multiple Forces. *J. Org. Chem.* **78**, 10344–10359.
52. Leriche, P., Frère, P., Cravino, A., Alévêque, O. and Roncali, J. (2007) Molecular engineering of the internal charge transfer in thiophene-triphenylamine hybrid  $\pi$ -conjugated systems. *J. Org. Chem.* **72**, 8332–8336. <https://doi.org/10.1021/jo701390y>.
53. Tang, X., Liu, W., Wu, J., Lee, C. S., You, J. and Wang, P. (2010) Synthesis, crystal structures, and photophysical properties of triphenylamine-based multicyno derivatives. *J. Org. Chem.* **75**, 7273–7278. <https://doi.org/10.1021/jo101456v>.
54. Li, Y., Ren, T. and Dong, W. J. (2013) Tuning photophysical properties of triphenylamine and aromatic cyano conjugate-based wavelength-shifting compounds by manipulating intramolecular charge transfer strength. *J. Photochem. Photobiol. A Chem.* **251**, 1–9. <https://doi.org/10.1016/j.jphotochem.2012.10.002>.
55. Pina, J., Seixas De Melo, J. S., Batista, R. M. F., Costa, S. P. G. and Raposo, M. M. M. (2013) Triphenylamine-benzimidazole derivatives: Synthesis, excited-state characterization, and DFT studies. *J. Org. Chem.* **78**, 11389–11395. <https://doi.org/10.1021/jo401803u>.
56. Sun, J., Sanow, L. P., Sun, S. S. and Zhang, C. (2013) Dicyano-substituted poly(phenylenevinylene) (DiCN-PPV) and the effect of cyano substitution on photochemical stability. *Macromolecules* **46**, 4247–4254. <https://doi.org/10.1021/ma400661f>.
57. Xia, D., Gehrig, D., Guo, X., Baumgarten, M., Laquai, F. and Müllen, K. (2015) A spiro-bifluorene based 3D electron acceptor with dicyanovinylene substitution for solution-processed non-fullerene organic solar cells. *J. Mater. Chem. A* **3**, 11086–11092. <https://doi.org/10.1039/C5TA00108K>.
58. Erande, Y. and Sekar, N. (2017) Enhanced NLO response in BODIPY-coumarin hybrids: density functional theory approach. *J. Chem. Sci.* **129**. <https://doi.org/10.1007/s12039-017-1340-0>.
59. Gupta, V. D., Tathe, A. B., Padalkar, V. S., Umape, P. G. and Sekar, N. (2013) Red emitting solid state fluorescent triphenylamine dyes: Synthesis, photo-physical property and DFT study. *Dye. Pigment.* **97**, 429–439. <https://doi.org/10.1016/j.dyepig.2012.12.024>.
60. Frisch, M. J., Trucks, G. W., Schlegel, H. B., Scuseria, G. E., Robb, M. A., Cheeseman, J. R., Scalmani, G., Barone, V., Mennucci, B., Petersson, G. A., Nakatsuji, H., Caricato, M., Li, X., Hratchian, H. P., Izmaylov, A. F., Bloino, J., Zheng, G., Sonnenberg, J. L., Hada, M., Ehara, M., Toyota, K., Fukuda, R., Hasegawa, J., Ishida, M., Nakajima, T., Honda, Y., Kitao, O., Nakai, H., Vreven, T., Montgomery, J. A., Peralta, J. E., Ogliaro, F., Bearpark, M., Heyd, J. J., Brothers, E., Kudin, K. N., Staroverov, V. N., Kobayashi, R., Normand, J.,

Raghavachari, K., Rendell, A., Burant, J. C., Iyengar, S. S., Tomasi, J., Cossi, M., Rega, N., Millam, J. M., Klene, M., Knox, J. E., Cross, J. B., Bakken, V., Adamo, C., Jaramillo, J., Gomperts, R., Stratmann, R. E., Yazyev, O., Austin, A. J., Cammi, R., Pomelli, C., Ochterski, J. W., Martin, R. L., Morokuma, K., Zakrzewski, V. G., Voth, G. A., Salvador, P., Dannenberg, J. J., Dapprich, S., Daniels, A. D., Farkas, Foresman, J. B., Ortiz, J. V., Cioslowski, J. and Fox, D. J. (2009) Gaussian 09, Revision B.01. *Gaussian 09, Revis. B.01, Gaussian, Inc., Wallingford CT.*

61. Cossi, M., Barone, V., Cammi, R. and Tomasi, J. (1996) Ab initio study of solvated molecules: a new implementation of the polarizable continuum model. *Chem. Phys. Lett.* **255**, 327–335. [https://doi.org/10.1016/0009-2614\(96\)00349-1](https://doi.org/10.1016/0009-2614(96)00349-1).

62. Tomasi, J., Benedetta Mennucci, A. and Cammi, R. (2005) Quantum Mechanical Continuum Solvation Models. *Chem. Rev.* **105**, 2999–3093. <https://doi.org/10.1021/CR9904009>.

63. Treutler, O. and Ahlrichs, R. (1995) Efficient molecular numerical integration schemes. *J. Chem. Phys.* **102**, 346–353. <https://doi.org/10.1063/1.469408>.

64. Becke, A. D. (1993) A new mixing of Hartree–Fock and local density-functional theories. *J. Chem. Phys.* **98**, 1372. <https://doi.org/10.1063/1.464304>.

65. Lee, C., Yang, W. and Parr, R. G. (1988) Development of the Colle–Salvetti correlation-energy formula into a functional of the electron density. *Phys. Rev. B* **37**, 785–789. <https://doi.org/10.1103/PhysRevB.37.785>.

66. Saranya, G., Kolandaivel, P. and Senthilkumar, K. (2011) Optical Absorption and Emission Properties of Fluoranthene, Benzo [ k ] fluoranthene, and Their Derivatives. A DFT Study. 14647–14656.

67. Hehre, W. J. (1976) Ab Initio Molecular Orbital Theory. **69**.

68. Bauernschmitt, R. and Ahlrichs, R. (1996) Treatment of electronic excitations within the adiabatic approximation of time dependent density functional theory. **2614**.

69. Tang, R. R. and Zhang, W. (2010) Facile procedure for the synthesis of 3-acetyl-9-ethylcarbazole and corresponding functionalized bis-diketone compounds. *Synth. Commun.* **40**, 601–606. <https://doi.org/10.1080/00397910903007095>.

70. Avula, V. K. R., Vallela, S., Anireddy, J. S. and Chamarthi, N. R. (2017) A Green Synthesis of 2-Amino-4-(9H-carbazole-3-yl)thiophene-3-carbonitriles by a Step-wise and One-pot Three-component Gewald Reaction. *J. Heterocycl. Chem.* **54**, 2471–2482. <https://doi.org/10.1002/jhet.2847>.

71. Ishi-i, T., Ikeda, K. and Kusakaki, Y. (2015) Light-emitting properties of donor–acceptor and donor–acceptor–donor dyes in solution, solid, and aggregated states: structure–property relationship of emission behavior. *RSC Adv.* **5**, 89171–89187. <https://doi.org/10.1039/c5ra18231j>.

72. Khanasa, T., Prachumrak, N., Rattanawan, R., Jungsuttiwong, S., Keawin, T., Sudyoasuk, T., Tuntulani, T. and Promarak, V. (2013) Bis(carbazol-9-ylphenyl)aniline End-Capped Oligoarylenes as Solution-Processed Nondoped Emitters for Full-Emission Color Tuning Organic Light-Emitting Diodes. *J. Org. Chem.* **78**. <https://doi.org/10.1021/jo4008332>.

73. Lockard, J. V, Ricks, A. B., Co, D. T. and Wasielewski, M. R. (2010) Interrogating the Intramolecular Charge-Transfer State of a Julolidine - Anthracene Donor - Acceptor Molecule with Femtosecond Stimulated Raman Spectroscopy. *J. Phys. Chem. Lett.* **1**, 215–218. <https://doi.org/10.1021/jz900136a>.
74. Haberhauer, G., Gleiter, R. and Burkhart, C. (2016) Planarized Intramolecular Charge Transfer : A Concept for Fluorophores with both Large Stokes Shifts and High Fluorescence Quantum Yields. *Chem. Eur. J.* **22**, 971–978. <https://doi.org/10.1002/chem.201503927>.
75. Liu, X., Xu, Z. and Cole, J. M. (2013) Molecular Design of UV – vis Absorption and Emission Properties in Organic Fluorophores : Toward Larger Bathochromic Shifts , Enhanced Molar Extinction Coefficients , and Greater Stokes Shifts. *J. Phys. Chem. C* **117**, 16584–16595. <https://doi.org/10.1021/jp404170w>.
76. Mcnamara, L. E., Liyanage, N., Peddapuram, A., Murphy, J. S., Delcamp, J. H. and Hammer, N. I. (2016) Donor–Acceptor–Donor Thienopyrazines via Pd-Catalyzed C–H Activation as NIR Fluorescent Materials. *J. Org. Chem.* **81**, 32–42. <https://doi.org/10.1021/acs.joc.5b01958>.
77. Pathak, A., Thomas, K. R. J., Singh, M. and Jou, J. (2017) Fine-Tuning of Photophysical and Electroluminescence Properties of Benzothiadiazole-Based Emitters by Methyl Substitution. *J. Org. Chem.* **82**, 11512–11523. <https://doi.org/10.1021/acs.joc.7b02127>.
78. Rajendra Kumar Konidena, K. R. Justin Thomas, Sudhir Kumar, Ya-Chi Wang, Chieh-Ju Li, and J.-H. J. (2015) Phenothiazine Decorated Carbazoles: Effect of Substitution Pattern on the Optical and Electroluminescent Characteristics. *J. Org. Chem.* **80**, 5812–5823. <https://doi.org/10.1021/acs.joc.5b00787>.
79. Guo, J., Li, X., Nie, H., Luo, W., Hu, R., Qin, A., Zhao, Z., Su, S. and Tang, B. Z. (2017) Robust Luminescent Materials with Prominent Aggregation-Induced Emission and Thermally Activated Delayed Fluorescence for High- Performance Organic Light-Emitting Diodes. *Chem. Mater.* **29**, 3623–3631. <https://doi.org/10.1021/acs.chemmater.7b00450>.
80. Beens, H., Knibbe, H. and Weller, a. (1967) Dipolar nature of molecular complexes formed in the excited state. *J. Chem. Phys.* **47**, 1183–1184. <https://doi.org/10.1063/1.1712006>.
81. Lippert, E., Rettig, W., Bonacic-koutecky, V., Heisel, F. and Miehle, J. A. (1987) Photophysics of internal twisting. *Adv. Chem. Phys.* **68**, 1–173. <https://doi.org/10.1002/9780470142967.ch1>.
82. Grabowski, Z. R., Rotkiewicz, K. and Rettig, W. (2003) Structural Changes Accompanying Intramolecular Electron Transfer: Focus on Twisted Intramolecular Charge-Transfer States and Structures. *Chem. Rev.* **103**, 3899–4031. <https://doi.org/10.1021/cr940745l>.
83. Kleinman, D. a. (1962) Nonlinear dielectric polarization in optical media. *Phys. Rev.* **126**, 1977–1979. <https://doi.org/10.1103/PhysRev.126.1977>.
84. Bilot, L. and Kawski, A. (1962) Zur Theorie des Einflusses von Lösungsmitteln auf die Elektronenspektren der Moleküle. *Zeitschrift Naturforsch. Tl. A* **17a**, 621–627.
85. Kawski, A. (2002) On the Estimation of Excited-State Dipole Moments from

Solvatochromic Shifts of Absorption and Fluorescence Spectra. *Zeitschrift Fur Naturforsch - Sect A J Phys Sci* **57**, 255–262.

86. Bakhshiev, N. G., Knyazhanskii, M. I., Osipov, V. I. M. O. A. and Saidov, G. V Experimental Determination of the Dipole Moments of Organic Molecules in Excited Electronic Experimental Determination of the Dipole Moments of Organic Molecules in Excited Electronic Statesf. **740**.

87. Liptay, W. (1965) Die lösungsmittelabhängigkeit der wellenzahl von elektronenbanden und die chemisch-physikalischen grundlagen. *Zeitschrift fur Naturforsch. - Sect. A J. Phys. Sci.* **20**, 1441–1471. <https://doi.org/10.1515/zna-1965-1109>.

88. Yu, L., Xi, J., Chan, H. T., Su, T., Antrobus, L. J., Tong, B., Dong, Y., Chan, W. K. and Phillips, D. L. (2013) Novel Organic D -  $\pi$ -2A Sensitizer for Dye Sensitized Solar Cells and Its Electron Transfer Kinetics on TiO<sub>2</sub> Surface. *J. Phys. Chem. C* **117**, 2041–2052. <https://doi.org/10.1021/jp3113182>.

89. Bodedla, G. B., Thomas, K. R. J., Fan, M. and Ho, K. (2016) Bi-anchoring Organic Dyes that Contain Benzimidazole Branches for Dye-Sensitized Solar Cells : Effects of p Spacer and Peripheral Donor Groups. *Chem. Asian J.* **11**, 2564–2577. <https://doi.org/10.1002/asia.201600766>.

90. Mohbiya, D. R. and Sekar, N. (2018) Tuning ‘Stokes Shift’ and ICT Character by Varying the Donor Group in Imidazo[1,5 a]pyridines: A Combined Optical, DFT, TD-DFT and NLO Approach. *ChemistrySelect* **3**, 1635–1644. <https://doi.org/10.1002/slct.201702579>.

91. Wu, W.-R. (2015) Theoretical investigation on the excited-state intramolecular proton transfer mechanism of 2-(2'-benzofuryl)-3-hydroxychromone. *J. Phys. Org. Chem.* **28**, 596–601. <https://doi.org/10.1002/poc.3455>.

92. Avhad, K., Jadhav, A. and Sekar, N. (2017) Fluorescent vinyl and styryl coumarins: A comprehensive DFT study of structural, electronic and NLO properties. *J. Chem. Sci.* **129**, 1829–1841. <https://doi.org/10.1007/s12039-017-1392-1>.

93. Glendening, E. D., Reed, A. E., Carpenter, J. E. and Weinhold, F. NBO Version 3.1. *NBO Version 3.1*.

94. Tabti, C. and Benhalima, N. (2015) Molecular Structure , Vibrational Assignments and Non-Linear Optical Properties of by DFT and ab Initio HF Calculations. *Adv. Mater. Phys. Chem.* **5**, 221–228.

95. Adant, C., Dupuis, M. and Bredas, J. L. (1995) Ab initio study of the nonlinear optical properties of urea: Electron correlation and dispersion effects. *Int. J. Quantum Chem.* **56**, 497–507. <https://doi.org/10.1002/qua.560560853>.

96. Momicchioli, F., Ponterini, G. and Vanossi, D. (2008) First- and second-order polarizabilities of simple merocyanines. An experimental and theoretical reassessment of the two-level model. *J. Phys. Chem. A* **112**, 11861–11872. <https://doi.org/10.1021/jp8080854>.

97. Abbotto, A., Beverina, L., Bradamante, S., Facchetti, A., Klein, C., Pagani, G. a., Redi-abshiro, M. and Wortmann, R. (2003) A distinctive example of the cooperative interplay of structure and environment in tuning of intramolecular charge transfer in second-order nonlinear optical chromophores. *Chem. - A Eur. J.* **9**, 1991–2007.

<https://doi.org/10.1002/chem.200204356>.

98. Castet, F., Pic, A. and Champagne, B. (2014) Linear and nonlinear optical properties of arylvinylidiazine dyes: A theoretical investigation. *Dye. Pigment.* **110**, 256–260. <https://doi.org/10.1016/j.dyepig.2014.03.021>.

99. Liyanage, P. S., De Silva, R. M. and De Silva, K. M. N. (2003) Nonlinear optical (NLO) properties of novel organometallic complexes: High accuracy density functional theory (DFT) calculations. *J. Mol. Struct. THEOCHEM* **639**, 195–201. <https://doi.org/10.1016/j.theochem.2003.08.009>.

100. Oudar, J. L. and Chemla, D. S. (1977) Hyperpolarizabilities of the nitroanilines and their relations to the excited state dipole moment. *J. Chem. Phys.* **66**, 2664–2668. <https://doi.org/10.1063/1.434213>.

101. Kwon, O., Jazbinsek, M., Seo, J., Kim, P., Choi, E., Sup, Y. and Günter, P. (2010) First hyperpolarizability orientation in asymmetric pyrrole-based polyene chromophores. *Dye. Pigment.* **85**, 162–170. <https://doi.org/10.1016/j.dyepig.2009.10.019>.

102. Cbeng, L., Tam, W., Stevenson, S. H., Meredith, G. R. and Marder, S. R. (1991) Experimental Investigations of Organic Molecular Nonlinear Optical Polarizabilities . 1 . Methods and Results on Benzene and Stilbene Derivatives. *J. Phys. Chem.* **95**, 10631–10643.

103. Yamashita, M., Kikuma, S., Yamaoka, Y., Murakami, H., Morita, R. and Shigekawa, H. (1999) Nonresonant femtosecond second hyperpolarizabilities of intramolecular charge-transfer molecules with great excited- and ground-state dipole-moment differences. *Appl. Phys. Lett.* **75**, 28. <https://doi.org/10.1063/1.124266>.

104. Isborn, C. M., Leclercq, A., Vila, F. D., Dalton, L. R., Brédas, J. L., Eichinger, B. E. and Robinson, B. H. (2007) Comparison of static first hyperpolarizabilities calculated with various quantum mechanical methods. *J. Phys. Chem. A* **111**, 1319–1327. <https://doi.org/10.1021/jp064096g>.

105. Thorat, K. G. and Sekar, N. (2017) Pyrrole-thiazole based push-pull chromophores: An experimental and theoretical approach to structural, spectroscopic and NLO properties of the novel styryl dyes. *J. Photochem. Photobiol. A Chem.* **333**, 1–17. <https://doi.org/10.1016/j.jphotochem.2016.10.009>.

106. Bhagwat, A. A., Avhad, K. C., Patil, D. S. and Sekar, N. (2018) Design and Synthesis of Coumarin-Imidazole Hybrid Chromophores: Solvatochromism, Acidochromism and Nonlinear Optical Properties. <https://doi.org/10.1111/php.13024>.

107. Deckers, S., Vandendriessche, S., Cornelis, D., Monnaie, F., Koeckelberghs, G., Asselberghs, I., Verbiest, T. and Van Der Veen, M. A. (2014) Poly(3-alkylthiophene)s show unexpected second-order nonlinear optical response. *Chem. Commun.* **50**, 2741–2743. <https://doi.org/10.1039/c3cc48099b>.

108. Meyers, F., Marder, S. R., Pierce, B. M. and Brédas, J. L. (1994) Electric Field Modulated Nonlinear Optical Properties of Donor-Acceptor Polyenes: Sum-Over-States Investigation of the Relationship between Molecular Polarizabilities ( $\alpha$ ,  $\beta$ , and  $\gamma$ ) and Bond Length Alternation. *J. Am. Chem. Soc.* **116**, 10703–10714. <https://doi.org/10.1021/ja00102a040>.

109. Kuzyk, M. G. (2006) Fundamental limits of all nonlinear-optical phenomena that are representable by a second-order nonlinear susceptibility. *J. Chem. Phys.* **125**, 1–11. <https://doi.org/10.1063/1.2358973>.

110. Katariya, S., Rhyman, L., Alswaidan, I. A., Ramasami, P. and Sekar, N. (2017) Triphenylamine-Based Fluorescent Styryl Dyes: DFT, TD-DFT and Non-Linear Optical Property Study. *J. Fluoresc.* **27**, 993–1007. <https://doi.org/10.1007/s10895-017-2034-1>.

111. C. Gayathri, A. R. (2008) Z -scan determination of the third-order optical nonlinearities of an azo dye using diode-pumped Nd:Yag laser. *Optik (Stuttg.)* **119**, 409–414. <https://doi.org/10.1016/j.ijleo.2006.12.011>.

112. Erande, Y., Kothavale, S., Sreenath, M. C., Chitrambalam, S., Joe, I. H. and Sekar, N. (2017) NLOphoric multichromophoric auxiliary methoxy aided triphenylamine D- p -A chromophores e Spectroscopic and computational studies. *Opt. Mater. (Amst.)* **73**, 602–616. <https://doi.org/10.1016/j.optmat.2017.09.017>.

113. Goel, N. and Kumar, B. (2012) Remarkable enhancement in optical and thermal properties of sodium hydrogen phthalate hemihydrate crystals due to Fe<sup>3+</sup> doping. *J. Cryst. Growth* **361**, 44–50. <https://doi.org/10.1016/j.jcrysgr.2012.08.044>.

114. Bhar, G. C. and Chaudhary, A. K. (2004) A comparative study of laser-induced surface damage thresholds in BBO crystals and effect of impurities. *Opt. Mater. (Amst.)* **27**, 119–123. <https://doi.org/10.1016/j.optmat.2004.02.027>.

115. Jiang, M., Gu, X., Lam, J. W. Y., Zhang, Y., Kwok, R. T. K., Wong, K. S. and Tang, B. Z. (2017) Two-photon AIE bio-probe with large Stokes shift for specific imaging of lipid droplets. *Chem. Sci.* **8**, 5440–5446. <https://doi.org/10.1039/C7SC01400G>.

## FIGURE CAPTIONS

**Figure 1.** The molecular structure of the previously reported analogue **1** and **5a-c** along with the daylight and UV-light photographs.

**Figure 2.** (a) Normalized absorption and (b) normalized emission graphs of **5a-c** in toluene.

**Figure 3.** (a)Weller plot and (b) Rettig's plot of **5a-c** in different solvents. The line corresponds to the best linear fit to the data.

**Figure 4.** Optimized S<sub>0</sub> geometries of **5a-c** in DMSO at the B3LYP/6-311++G(d,p) level. Note: C atoms = Black color, H atoms = green color and N atoms = Blue color.

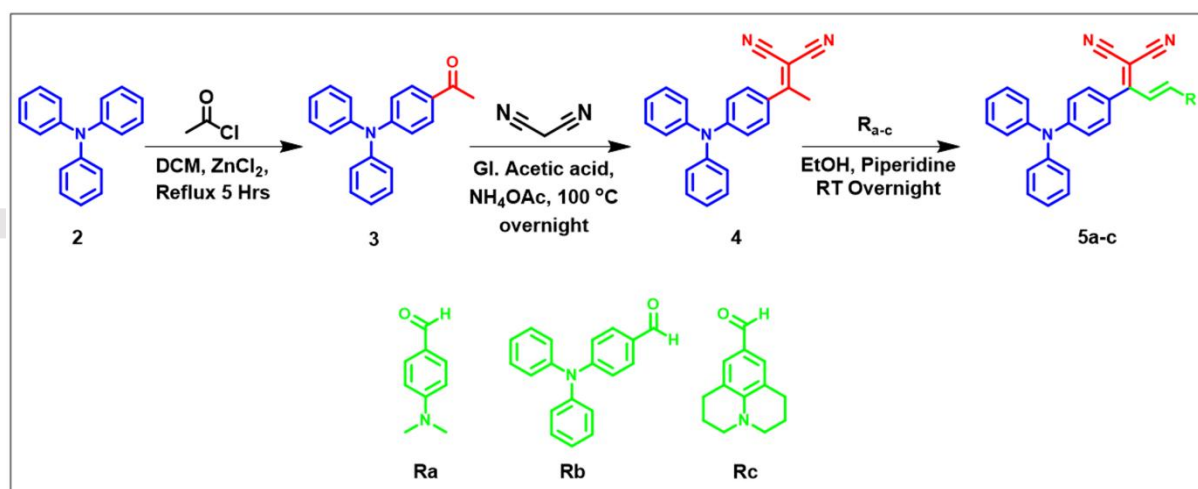
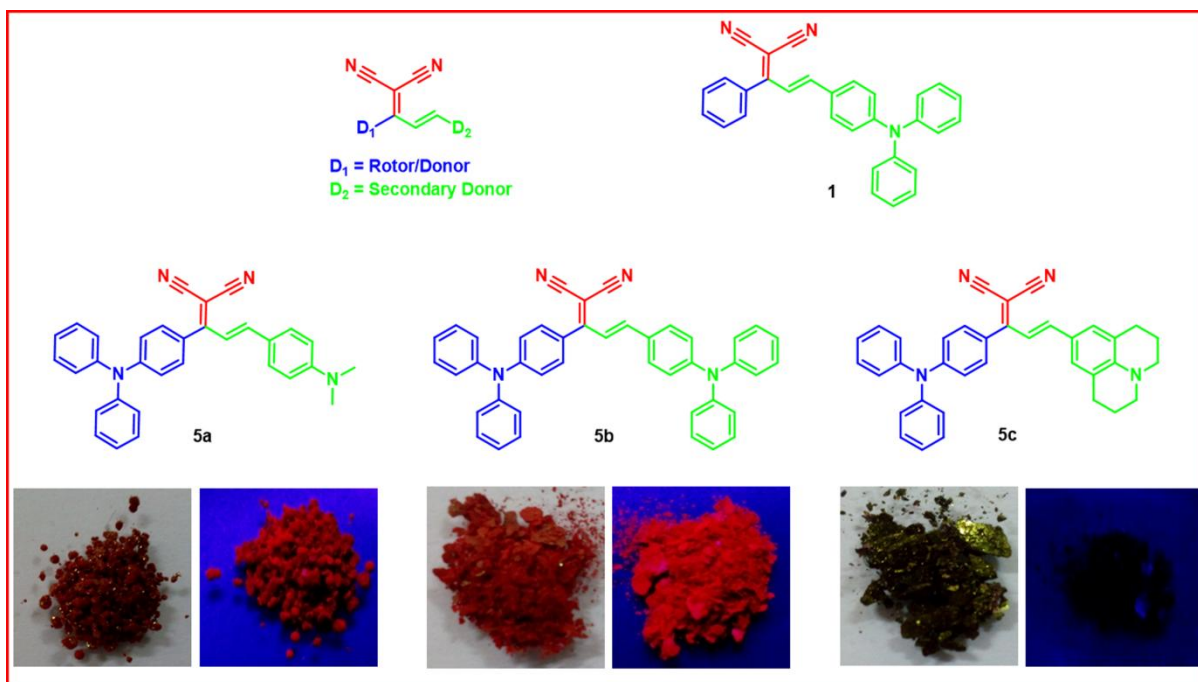
**Figure 5.** Electronic distribution of the selected molecular orbitals for the dyes **5a-c**.

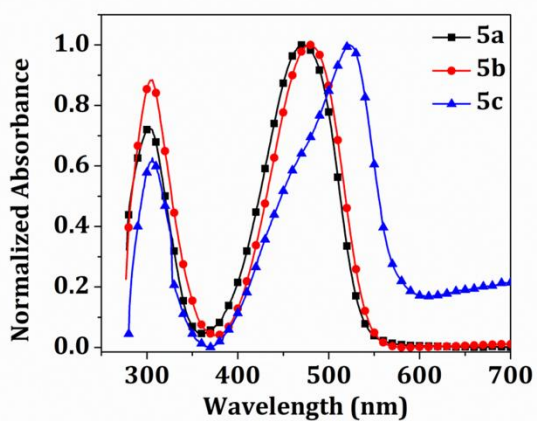
**Figure 6.** (a) BLA vs. hyperpolarizability (by RSH functional) of dyes **5a-c**. (b) BOA vs. hyperpolarizability (by RSH functional) of dyes **5a-c**.

**Figure 7.** (a) Normalized closed aperture Z-scan curve and (b) normalized open aperture Z-scan curve for dyes **5a-c**.

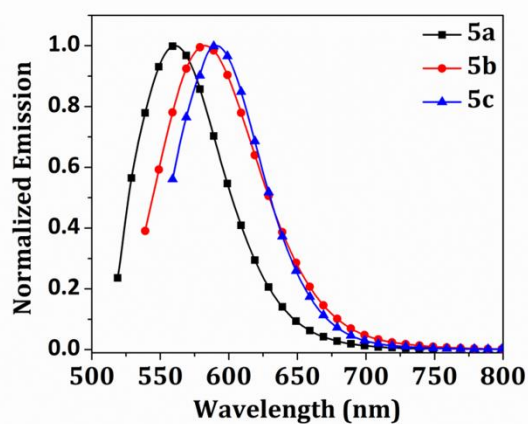
**Figure 8.** Optical Limiting (OL) Plot of dyes **5a** and **5b** in the respective solvents.

**Figure 9.** Optical limiting curve plotted as input fluence vs. transmittance. Optical limiting values for **5a** and **5b** in acetone were found to be 17.20 and 9.55 Jcm<sup>-2</sup> respectively, whereas in ethanol it was 6.43 Jcm<sup>-2</sup> for **5b**.

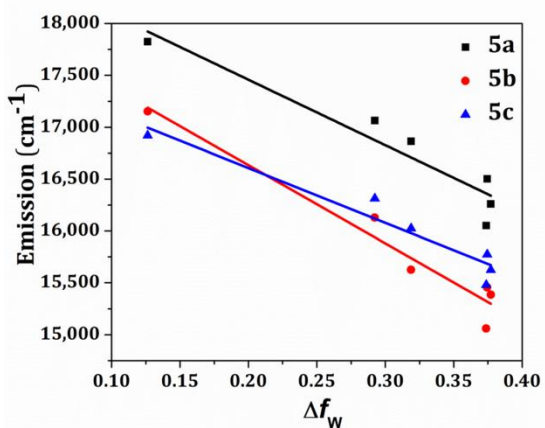




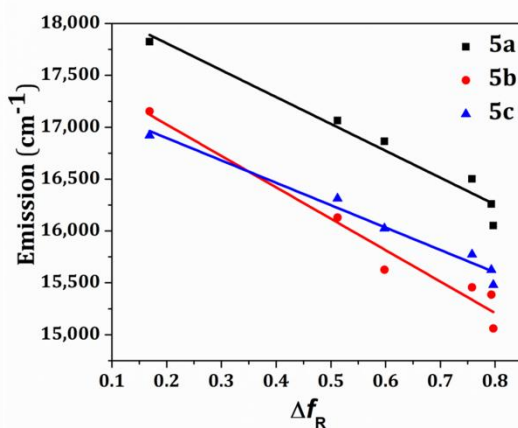
(a)



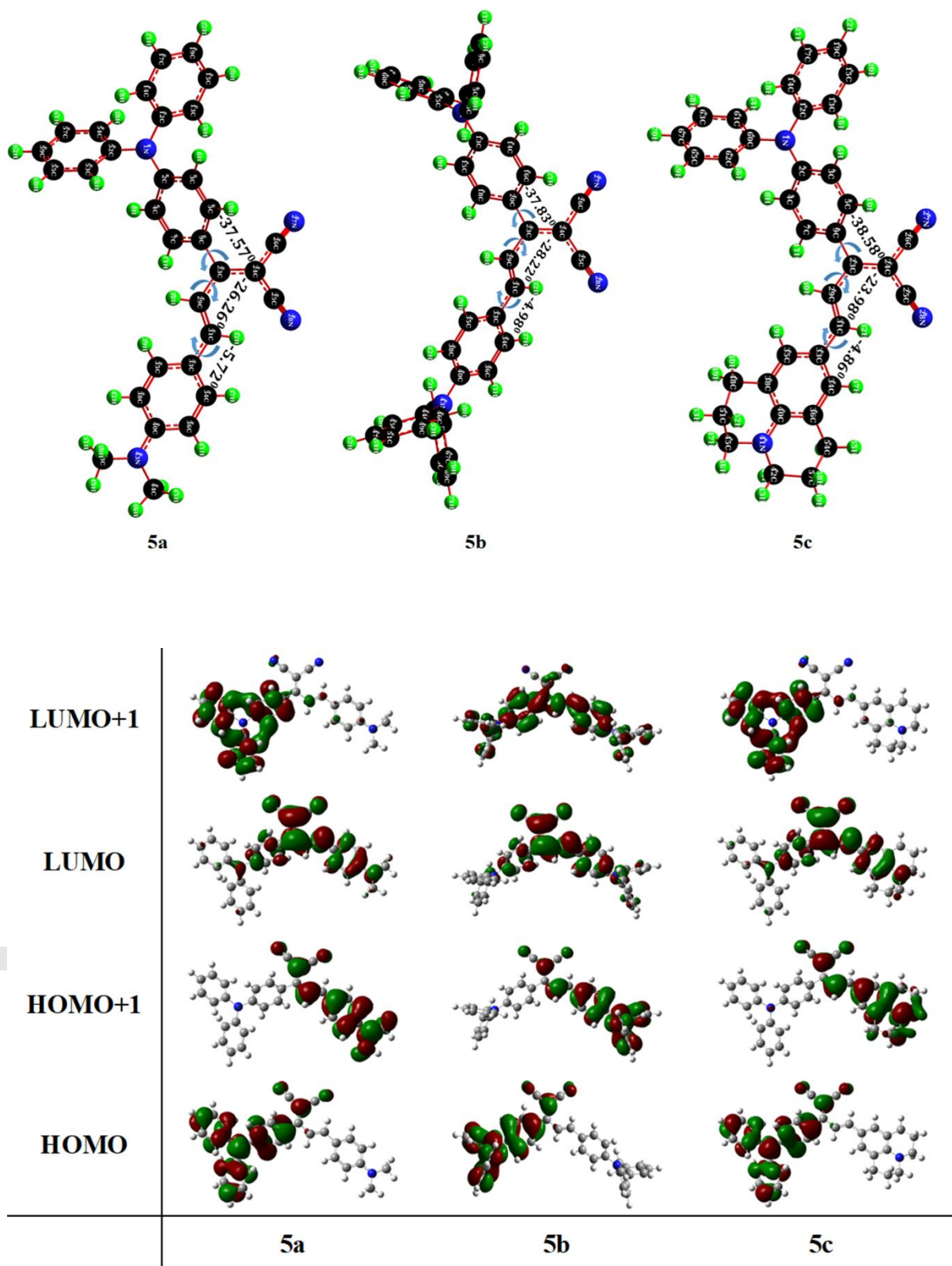
(b)

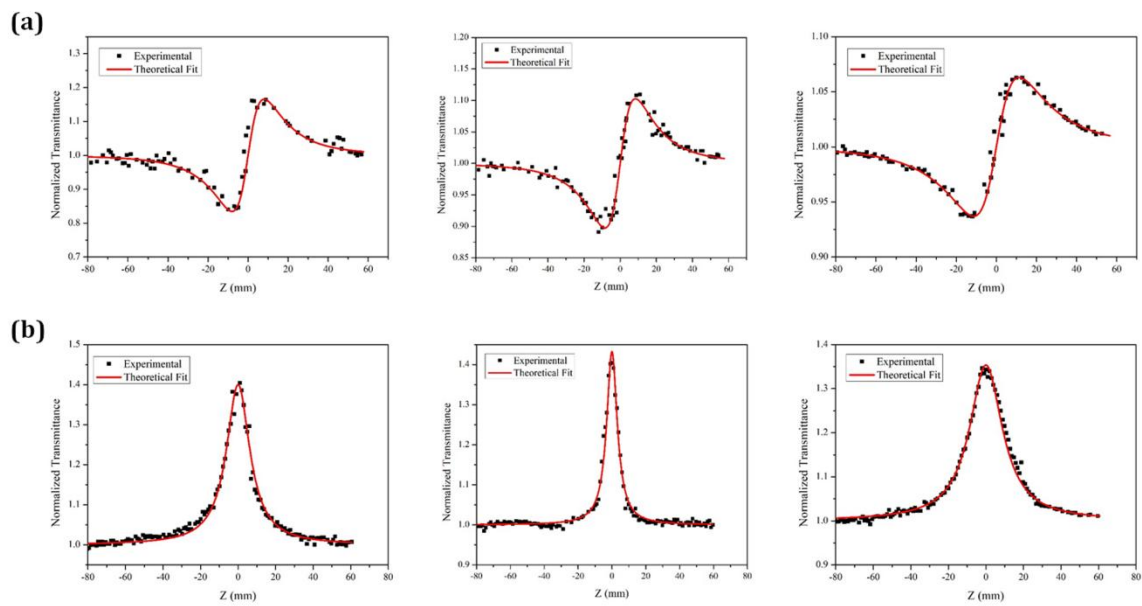
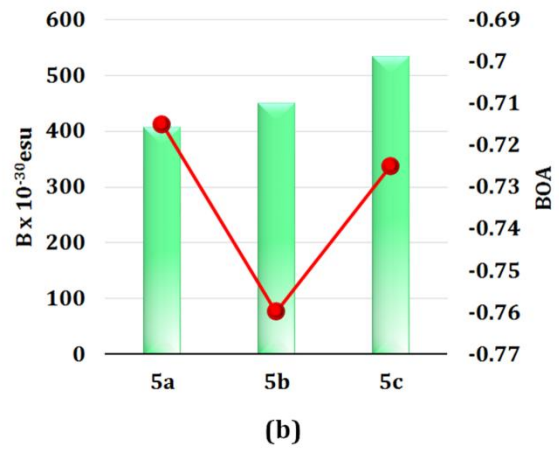
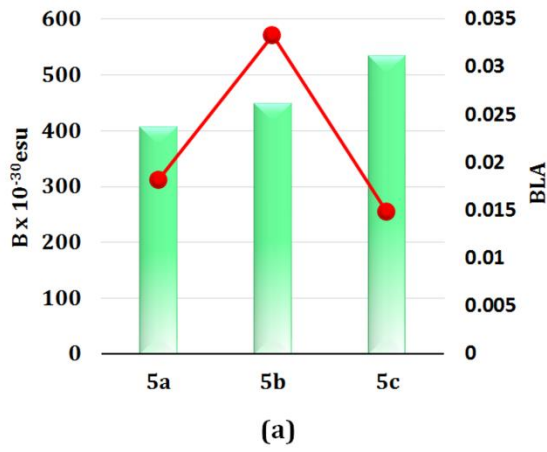


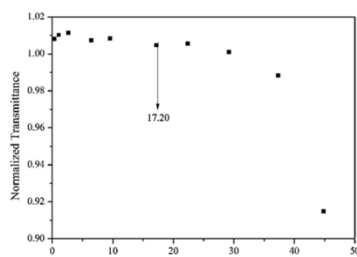
(a)



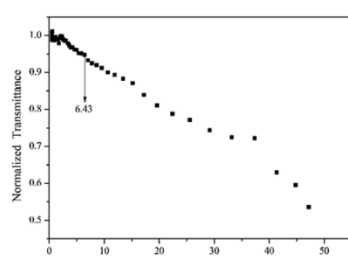
(b)



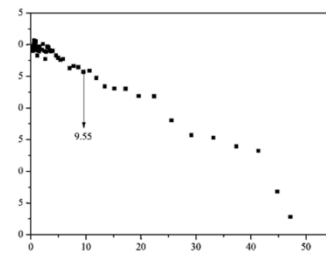




Acetone  
(5a)



Ethanol



Acetone

(5b)